Spectroscopy of Atomic Zinc Inside a Heat Pipe: Towards Resonance Ionisation

by

Brandon Dane Hattingh

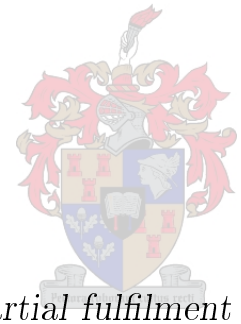

Thesis presented in partial fulfilment of the requirements for the degree of Master of Science in Laser Physics in the Physics Department at Stellenbosch University

Supervisor: Dr. Christine Steenkamp

April 2019

Declaration

By submitting this thesis electronically, I declare that the entirety of the work contained therein is my own, original work, that I am the sole author thereof (save to the extent explicitly otherwise stated), that reproduction and publication thereof by Stellenbosch University will not infringe any third party rights and that I have not previously in its entirety or in part submitted it for obtaining any qualification.

Date: April 2019

Abstract

Spectroscopy of Atomic Zinc Inside a Heat Pipe: Towards Resonance Ionisation

B.D. Hattingh

Department of Physics,
Stellenbosch University,
Private Bag X1, Matieland 7602, South Africa.

Thesis: Masters

April 2019

Zinc (Zn) reserves in South Africa are not being used to full potential. Separating Zn into its different stable isotopes drastically increases its value, as well as usefulness in certain areas such as research, industry and medicine, for example, ^{68}Zn is a precursor of ^{68}Ga used for Positron-Emission Tomography/Computed Tomography (PET/CT) scans to detect tumours. This project aims to develop a complementary experimental setup and computational model in aid of a larger project that aims to develop an efficient and feasible laser-based process to separate Zn isotopes. Time-delayed-reference-beam Atomic Absorption Spectroscopy (AAS) inside a heat pipe is used to optimise experimental parameters. Computationally, Einstein rate equations are used to describe the interaction of atoms with the incident laser beam. The avialable pulsed dye laser provides pulses of 8 ns duration and peak intensity of 7.5×10^8 W/m^2.

Using the Einstein rate equations, it is found that, for the dipole allowed $4s^2\ ^1S_0 \rightarrow 4s4p\ ^1P_1{}^o$ transition, 5 ps is needed for the population of the energy levels to reach a steady state with a constant laser intensity of 7.5×10^8 W/m^2. The peak intensity needed to saturate this transition when using a pulse with Gaussian temporal envelope and FWHM of 8 ns is 2×10^7 W/m^2. For the dipole forbidden $4s^2\ ^1S_0 \rightarrow 4s4p\ ^3P_1{}^o$ transition, 30 ns is needed to reach a steady state with a constant laser intensity of 7.5×10^8 W/m^2. When using a Gaussian pulse with a FWHM of 8 ns, a peak intensity of more than 7.5×10^8 W/m^2 is needed to saturate this transition. For the $4s^2\ ^1S_0 \rightarrow 4s4p\ ^1P_1{}^o$ transition, the absorption cross-section is found to be $\sigma = 3.3 \times 10^{-16}$ m^2, using a general equation derived from the rate equations. Moreover, it is found that a temperature of 668 K for the Zn atoms is needed for 50% absorption in the heat pipe, when using an intensity of 7.5×10^8 W/m^2. Experimentally, the measured absorption line was found to have a spectral FWHM of 0.4 nm, which is large compared to the simulated spectral FWHM of 0.0025 nm. The broadening is likely due to power broadening and broadening due to collisions, which

is not accounted for in the computational model. Improved conditions, that should be implemented when using the setup in the future, were derived from the combined experimental and computational results.

Uittreksel

Spektroskopie van Sink-Atome in 'n Hittepyp: In Voorbereiding vir Resonans Ionisasie

("Spectroscopy of Atomic Zinc Inside a Heat Pipe: Towards Resonance Ionisation")

B.D. Hattingh

Departement Fisika,
Stellenbosch Universiteit,
Privaatsak X1, Matieland 7602, Suid Afrika.

Tesis: Meesters

April 2019

Die sink (Zn) reserwes in Suid-Afrika word nie tot volle potensiaal benut nie. Die skeiding van die verskillende stabiele Zn isotope van mekaar sal die waarde, sowel as die bruikbaarheid in velde soos navorsing, industrie en medisyne, drasties verhoog. ^{68}Zn is byvoorbeeld 'n voorloper van ^{68}Ga wat gebruik word vir Positron-Emissie Tomografie/Rekenaartomografie (PET/CT) skanderings om kanker op te spoor.

Hierdie projek se doel is om 'n komplementêre eksperimentele opstelling en numeriese model te ontwikkel wat van hulp sal wees 'n in groter projek waarvan die doel is om 'n doeltreffende en haalbare laser-gebaseerde proses te ontwikkel om Zn isotope te skei. Tyd-vertraagde-verwysingsbundel Atoom Absorpsie Spektroskopie (AAS) in 'n hittepyp word gebruik om die eksperimentele parameters te optimeer. In die numeriese model word die Einstein koersvergelykings gebruik om die interaksie van die atome met die inkomende laserbundel te beskryf. Die beskikbare laser lewer pulse van 8 ns duur met 'n piekintensiteit van 7.5×10^8 W/m^2.

Deur die gebruik van die Einstein koersvergelykings word gevind dat, vir die dipool-toegelate $4s^2\ ^1S_0 \rightarrow 4s4p\ ^1P_1{}^o$ oorgang, 5 ps nodig is vir die bevolking van die energievlakke om 'n ewewigstoestand te bereik met 'n konstante laser intensiteit van 7.5×10^8 W/m^2. Die piekintensiteit wat nodig is om hierdie oorgang te versadig wanneer 'n laserpuls met 'n Gaussiese tydprofiel en 'n volle-wydte-by-half-maksimum van 8 ns gebruik word is 2×10^7 W/m^2. Vir die dipool-verbode $4s^2\ ^1S_0 \rightarrow 4s4p\ ^3P_1{}^o$ oorgang is 30 ns nodig om 'n ewewigstoestand te bereik met 'n konstante laser intensiteit van 7.5×10^8 W/m^2. Wanneer 'n Gaussiese puls met 'n wydte van 8 ns gebruik word is 'n piekintensiteit van meer as 7.5×10^8 W/m^2 nodig om die oorgang te versadig. Vir die dipool-toegelate $4s^2\ ^1S_0 \rightarrow 4s4p\ ^1P_1{}^o$ oorgang is die absorpsiedeursnit bepaal as $\sigma = 3.3 \times 10^{-16}$ m^2 deur gebruik te maak van 'n algemene uitdrukking, wat afgelei is

van die koersvergelykings. Verder is daar gevind dat 'n temperatuur van 668 K vir die Zn atome nodig is om 50% absorpsie in die hittepyp te kry, wanneer 'n intensiteit van 7.5×10^8 W/m^2 gebruik word. In die eksperimentele metings is daar gevind dat die absorpsielyn 'n spektrale wydte van 0.4 nm het, wat groot is in vergelyking met die berekende spektrale wydte van 0.0025 nm. Die verbreding is waarskynlik die gevolg van versadiging en drukverbreding wat nie in ag geneem word in die numeriese model nie. Van die gekombineerde eksperimentele en numeriese resultate is verbeterde kondisies afgelei, wat gebruik behoort te word wanneer die opstelling in die toekoms aangewend word.

Acknowledgements

I would like give a special thanks to the people that supported me and made this project a success. I would first and foremost want to thank my family for their love and support. My supervisor, Dr. Christine Steenkamp, was remarkable in her attention to detail, uninterrupted in her support and dedication, without which this project would be impossible and I could not be more greatful. I would like to thank Frikkie Waso and Andre de Bruyn, my collegues in the spectroscopy labaratory, for their continual advice, support and comaraderie. I would like to give a special thanks to Henk Van Wyk from the CSIR for doing an outstanding job helping with the setup and alignment of the lasers as well as just being a pleasure to work with. I would also like thank the brilliant workshop, Mr. Gerhard Louwrens, Mr. Lawrence Ashworth, Mr. David Pool, Mr. Eben Shields, Mr. Johan Germishuizen and Mr. Hugh Esterhuizen for their help with designing and constructing critical components of the experimental setup. Last but not least I would like to thank the administrative staff at the physics department, Ms. Colleen April, Mrs. Elsebe Bosch, Mr. Stanley February, Mr. Tinus Botha, Mr. Cashwell Pool and Mrs. Ursula Isaacs for going above and beyond the call of duty.

Dedications

For my family.

Vir my familie.

Contents

List of Figures

1. Introduction

South Africa has the 31st highest production of zinc (Zn) concentrate in the world at 26 695 metric tons in 2016 [5]. The mining process of Zn begins with the mining of natural ore. Once the ore is mined, a concentrate is produced which contains roughly 50% Zn content. Further refinement is needed for pure Zn (99.995%), which is used in zinc's most used case, hot-dip galvanising, which protects metals from rust. Even further refinement is needed to separate Zn into different isotopes. Zn isotopes are high value products, but Zn isotope separation is not currently being done in South Africa. Consequently, South Africa's Zn reserves are not used to their full potential. Zn isotopes are useful in medicine, industry and research. An important medical use for pure Zn isotopes is the production of Ga-based radiopharmaceuticals for medical uses such as tumour detection [6; 7; 8].

This project forms part of a larger project which aims to develop an efficient and feasible laser-based process to separate Zn isotopes, specifically ^{68}Zn for use in Positron-Emission Tomography-Computed Tomography (PET/CT) scans and ^{67}Zn for use in Single-Photon Emission Computed Tomography (SPECT) scans [9].

For this project the focus will be on developing a complementary experimental setup and computational model that will be used to investigate ionization schemes for Zn and find the most efficient resonance ionisation scheme for particular physical conditions. In this project isotope separation will not be performed as the laser bandwidth used is not narrow enough. However, the properties of different isotopes for the same state are similar. These properties can be used to find to optimal ionisation scheme irrespective of isotope selectivity. Physical conditions will be investigated experimentally through Atomic Absorption Spectroscopy (AAS) in Zn vapour as well as computationally through an Einstein rate equation describing the behaviour of atoms with incident laser beams. The reason for using AAS instead of ion detection is beacuse in AAS it is possible to record the amount of absorbed light for each step of the ionisation scheme, which is not possible when only recording ion current.

To model a resonance ionisation scheme with two or more steps, not only the chosen excitation transitions are important, but all transitions involved in de-excitation paths back to lower states. A computer model is needed in order to interpret the experimental measurements (e.g. transition probability from a measurement) and to investigate the influence of experimental parameters that cannot be easily adjusted such as laser pulse duration. The computer model is also used to predict feasible experimental parameters such as the density of Zn vapour, intensity of laser beam and ionisation level scheme to be used in the current setup.

During this project a Zn heat pipe is commissioned to provide a homogeneous atomic vapour for AAS. The temperature, pressure and density of the Zn vapour inside the heat pipe are determined and investigated. A time-delayed-reference-beam absorption

spectroscopy setup, with frequency doubled dye laser beams and a single detector, is developed. Protocol and software are developed to analyse results of the time-delayed-reference-beam absorption spectroscopy. The first excitation step ($4s^2\ ^1S_0 \rightarrow 4s4p\ ^1P_1{}^o$) is detected and compared to simulated data. This transition is chosen as the first excitation step, because it has a large absorption cross-section due to it being an allowed state.

The Einstein rate equation model of a two level system is adapted to simulate and explore the population dynamics of the ground state ($4s4p\ ^1S_0$) and the first excited state ($4p^2\ ^1P_1{}^o$) of Zn. The time evolution of the laser pulse is introduced into the equation to simulate the interaction with 8 ns pulses.

From the rate equation theory, expressions for the absorption cross-sections and the absorption coefficients are derived and investigated.

Using the estimated density of the atoms, Doppler broadened transition bandwidth and laser frequency bandwidth in the rate equation model, the expected absorption percentage in the heat pipe is calculated and compared to experimental data.

The results from the rate equation model and the exprimental data are useful to optimise the conditions for an experiment that will be used in the future to evaluate and optimise resonance ionisation schemes for Zn.

2. Theory

2.1 Zinc

Natural Zn comprises of five stable isotopes, ^{64}Zn, ^{66}Zn, ^{67}Zn, ^{68}Zn and ^{70}Zn. ^{64}Zn is the most abundant isotope comprising 48% of natural Zinc [10]. The natural abundancies of Zinc are presented in Table 2.1 below.

Zinc Isotope	**Natural Abundance**
^{64}Zn	48.27%
^{66}Zn	27.98%
^{67}Zn	4.10%
^{68}Zn	19.02%
^{70}Zn	0.6%

Table 2.1: Abundancies of stable Zn isotopes in Natural Zn [10].

An abundance of research has been done in an attempt to understand the physics of atoms. The following will summarise some of the important findings with regards to the atomic structure of Zn.

The nucleus of Zn atoms contains 30 protons. The nucleus also contains 34 to 40 neutrons, which contributes to the standard atomic weight of 65.38 u, as per Table 2.1. The standard atomic weight reflects the difference in isotope masses in a natural sample of Zn.

Zn isotopes have many uses in industry, medicine and research. Uses of Zn isotopes in industry include the use of depleted zinc oxide (DZO) in ^{64}Zn in the cooling water of nuclear reactors to reduce radionuclides [11]. Uses in medicine include imaging tumours using Ga-68-DOTANOC Positron-Emission Tomography-Computed Tomography (PET/CT) scans [12], where Zn is transported and then stored, before producing Ga via the ^{68}Zn(p,n)^{68}Ga proton reaction. This reaction and other reactions for producing Ga from Zn are highlighted in the Nuclide Table extract, Figure 2.1 [6; 7; 8]. Among research in astronomy utilising zinc isotopes is the study of Gamow-Teller strength distribution in proton-rich nucleus ^{57}Zn [13].

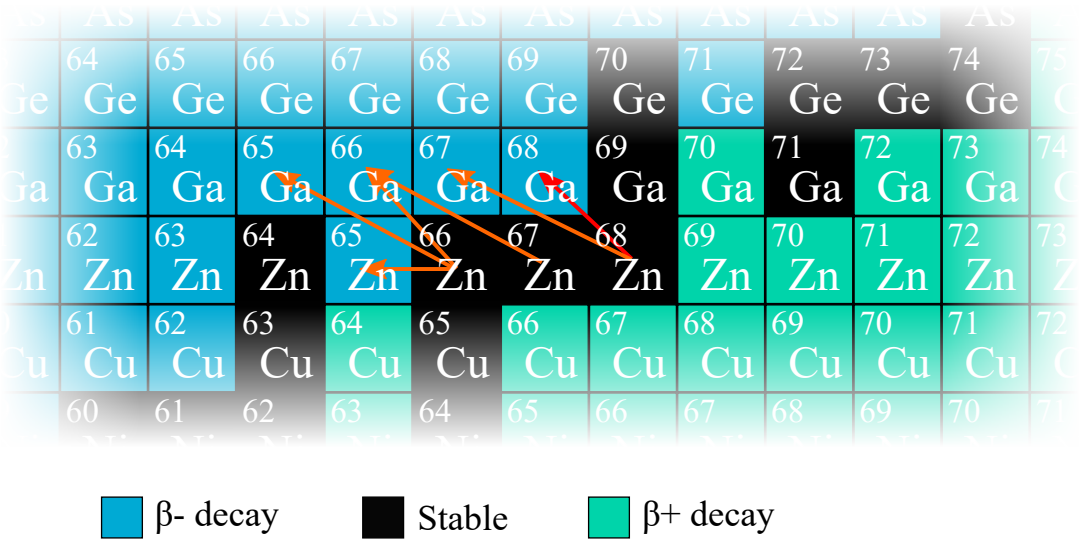

Figure 2.1: Extract from The Nuclide Table, highlighting ^{66}Zn(p,n)^{66}Ga, ^{66}Zn(p,n+p)^{65}Zn, ^{66}Zn(p,2n)^{65}Ga, ^{67}Zn(p,2n)^{66}Ga, ^{68}Zn(p,2n)^{67}Ga excitations are depicted in orange and the ^{68}Zn(p,n)^{68}Ga excitation in red. The image is produced by the author from information from The Live Nuclide Table [1].

2.1.1 Transition Rules

The LS Coupling Scheme will be used for Zn. This means that the individual orbital angular momenta, l, of each particle making up the atom are summed to find the total orbital angular momentum, L, of the atom. Similarly, for the spin, the individual spin angular momenta, s, of each particle making up the atom are summed to find the total spin angular momentum, S, of the atom. The total angular momentum, J, is the sum of the total orbital angular momentum, L, and the total spin angular momentum, S.

An example of the notation using the LS Coupling Scheme would be the singlet state, $3d^{10}\ 4s4p\ {}^1P_1{}^o$, where the total spin angular momentum of $S = 0$ is indicated in the superscript as $2S+1=1$, the total orbital angular momentum, $L = 1$ is indicated as the letter P (S, P, D, F, ... for $L = 1, 2, 3, 4, \ldots$) and the total angular momentum of $J = 1$ is indicated in the subscript.

The transition rules in Atomic Spectroscopy make it possible to distinguish between allowed and forbidden transitions. Allowed transitions have larger absorption cross-sections, shorter lifetimes and larger Einstein A coefficients compared to forbidden transitions. The Einstein A coefficient is the rate at which an atom that is in a specific excited state spontaneously decays to lower energy states. The Einstein B coefficient relates to the rate at which an atom that is in a specific state decays to lower energy state due to stimulated emission or excites to a higher excited state due to absorption. Allowed transitions have Einstein A coefficients in the order of 10^6 s^{-1} to 10^8 s^{-1} while forbidden states have Einstein A coefficients in the order of 10^4 s^{-1} or less [14].

For electric dipole transitions using LS coupling, there are 6 transition rules, summarised in Table 2.2 [15].

Transition Rules	
1.	$\Delta J = 0, \pm 1$, except $0 \not\leftrightarrow 0$
2.	$\Delta M = 0, \pm 1$, except $0 \not\leftrightarrow 0$ when $\Delta J = 0$
3.	Parity change
4.	$\Delta l = \pm 1$ and Δn arbitrary with one electron jumping
5.	$\Delta S = 0$
6.	$\Delta L = 0, \pm 1$, except $0 \not\leftrightarrow 0$

Table 2.2: Transition rules for electric dipole transitions using LS coupling [15].

2.2 Laser Isotope Separation by Resonance Ionisation

Resonance Ionisation Separation is the process of separating isotopes by resonantly and selectively exciting a specific isotope. It is done by tuning a laser beam to the first excitation energy of the specific isotope incident on the sample. The next step is to ionise the excited isotopes. The natural sample can be separated from a specific isotope. This is achieved by exerting an external electric field that will extract the now ionised isotopes.

Isotope energy levels are very close together, in the order of 0.01 cm^{-1}. Therefore a laser with a very narrow bandwidth needs to be used for the first excitation step. If the fringes of the laser beam profile overlap with the energy level of another isotope, an iterative process can be used, where each iteration will produce a product that is more pure.

The best ionisation scheme for zinc is not well known. More Resonance Ionisation Spectroscopy needs to done to find this scheme.

2.3 Resonance Ionisation Spectroscopy of Zinc

Resonance Ionisation Spectroscopy is used to find, study and investigate the most efficient ionisation scheme for zinc. The most efficient ionisation scheme will be the scheme that leads to the most zinc of a specific isotope being ionised with the smallest amount of other isotopes also being ionised.

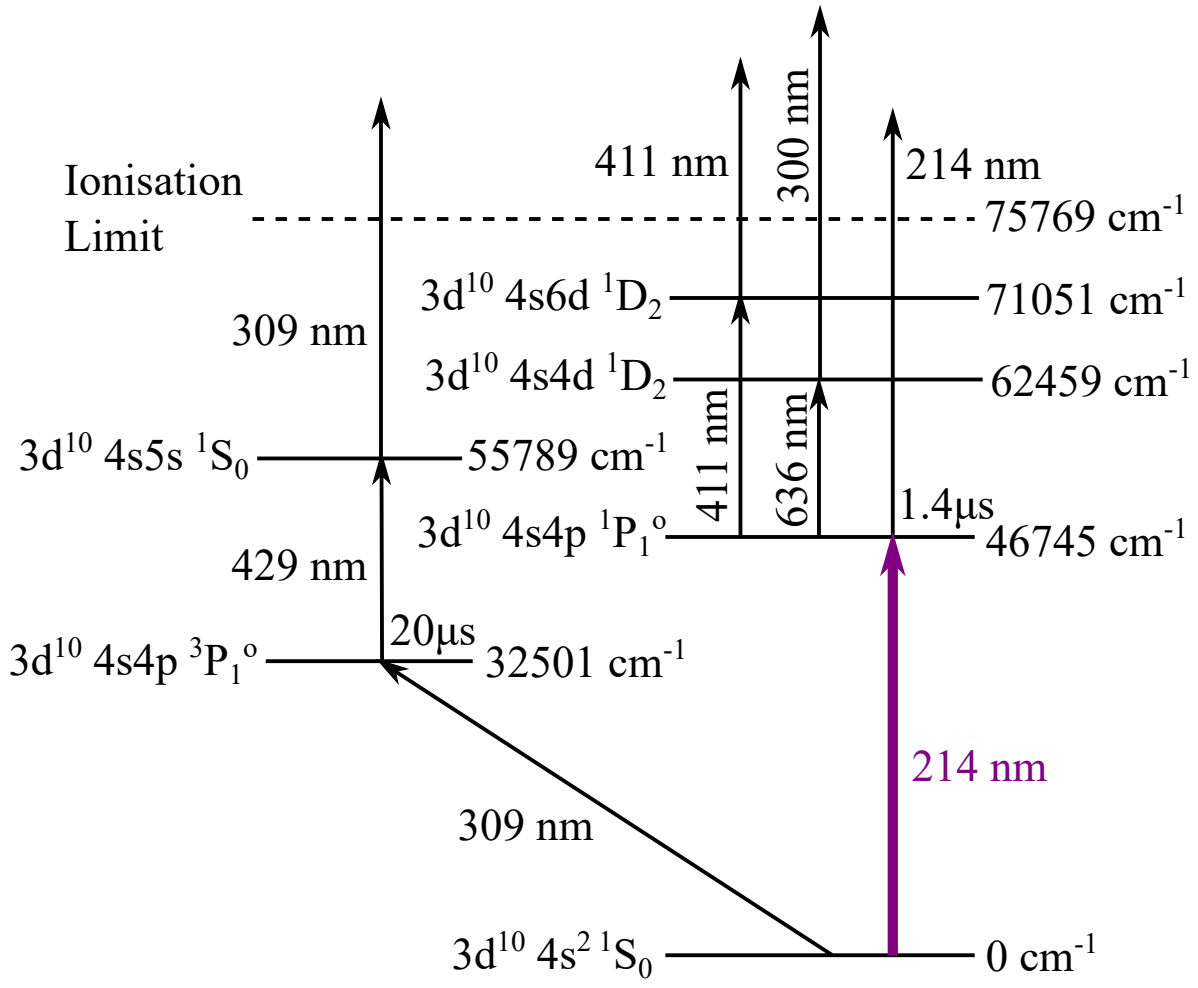

Figure 2.2: Example of a Resonance Ionisation scheme for zinc [2].

Saloman [2] has identified ionisation schemes used in the past. An example of ionisation schemes are shown in Figure 2.2 [2]. The purple highlighted excitation from the ground state $4s^2\ {}^1S_0$ to the excited state $4s4p\ {}^1P_1{}^o$ are investigated in the Results and Discussion, Section 4.

The step where the selection of a particular isotope occurs is in the first excitation. There are two main options for this first excitation, from the ground state, $4s^2\ {}^1S_0$, to the singlet state, $4s4p\ {}^1P_1{}^o$, and from the ground state, $4s^2\ {}^1S_0$, to the triplet state, $4s4p\ {}^3P_1{}^o$.

$$4s^2\ {}^1S_0 \rightarrow 4s4p\ {}^1P_1{}^o \qquad \textbf{OR} \qquad 4s^2\ {}^1S_0 \rightarrow 4s4p\ {}^3P_1{}^o$$

Both transitions have their advantages and disadvantages, as will be discussed in Section 2.3.1 and 2.3.2.

2.3.1 Singlet-Singlet Transition $4s^2\ ^1S_0 \rightarrow 4s4p\ ^1P_1{}^o$

The advantage of the singlet-singlet transition is that it is an allowed state. This is seen by using the transition rules described in Section 2.1.1, as summarised in Table 2.3. Allowed states have greater transition probabilities, which means a larger absorption cross-section. This means a lower power of resonant radiation is needed to saturate the transition and excite the maximal fraction of the population to the upper state.

Allowed or Forbidden	**Change**	**Description**
Allowed	$\mathbf{\Delta S = 0}$	There is no change in spin angular momentum. It is a singlet to singlet transition.
Allowed	$\mathbf{\Delta L = +1}$	There is a change in orbital angular momentum from L = 0 (S orbital) to L = 1 (P orbital).
Allowed	$\mathbf{\Delta J = +1}$	There is a change in total angular momentum J = 0 to J = 1.
Allowed	**Even $\rightarrow$ Odd**	There is a change in parity from even to odd.

Table 2.3: Transition rules for the singlet-singlet transition $4s^2\ ^1S_0 \rightarrow 4s4p\ ^1P_1{}^o$.

One of the disadvantages is that the state has a short lifetime of 1.4 ns [16] compared to the singlet-triplet transition with a lifetime of 20 μs [16]. This means that the temporal window that is available to ionise isotopes from the $4s4p\ ^1P_1{}^o$ state is very small. Another disadvantage is that the isotope shifts between the different isotopes are smaller, as can be seen in Table 2.4. This means that either a very narrowband laser may be used in conjunction with experimental conditions where line broadening mechanisms are avoided or a multiple iteration approach may be attempted, depending on the purity needed.

Transition	^{64}Zn	^{66}Zn	^{67}Zn	^{68}Zn
$4s^2\ ^1S_0 \rightarrow 4s4p\ ^1P_1{}^o$	0	0.018 cm^{-1}	unmeasured	0.033 cm^{-1}
$4s^2\ ^1S_0 \rightarrow 4s4p\ ^3P_1{}^o$	0	0.022 cm^{-1}	unmeasured	0.045 cm^{-1}

Table 2.4: Isotope shifts for different zinc isotopes from Saloman 1989 [2].

2.3.2 Singlet-Triplet Transition $4s^2\ ^1S_0 \rightarrow 4s4p\ ^3P_1{}^o$

The main disadvantage of the triplet transition is that it is a forbidden state, as shown in Table 2.5, using the rules described in Section 2.1.1. This results in a smaller transition probability, which means a smaller absorption cross-section. Thus a higher power

of resonant radiation is needed to saturate the transition and excite the maximal fraction of the population to the upper state.

Allowed or Forbidden	**Change**	**Description**
Forbidden	$\mathbf{\Delta S = +1}$	There is a change in spin angular momentum from S = 0 (singlet) to S = 1 (triplet).
Allowed	$\mathbf{\Delta L = +1}$	There is a change in orbital angular momentum from L = 0 (S orbital) to L = 1 (P orbital).
Allowed	$\mathbf{\Delta J = +1}$	There is a change in total angular momentum of $\Delta J = 1$, for the $^1S_0 \rightarrow {}^3P_1{}^o$ transition. The other two transitions, $^1S_0 \rightarrow {}^3P_0$ and $^1S_0 \rightarrow {}^3P_2$, are forbidden, because $J = 0 \rightarrow J = 0$ for $^1S_0 \rightarrow {}^3P_0$ and $\Delta J = 2$ for $^1S_0 \rightarrow {}^3P_2$.
Allowed	**Even $\rightarrow$ Odd**	There is a change in parity from even to odd.

Table 2.5: Transition rules for the singlet-triplet transition $4s^2\ {}^1S_0 \rightarrow 4s4p\ {}^1P_1{}^o$.

One of the advantages is that the state has the long lifetime of 20 μs [16] compared to the singlet-singlet transition which has a lifetime of 1.4 ns [16]. This means that the temporal window that is available to ionise isotopes from the 4s4p $^3P_1{}^o$ state is in the order of 20 μs. Another advantage is that the isotope shifts between the different isotopes are larger, as can be seen in Table 2.4. This means that, given a laser with a certain bandwidth, greater isotope selectivity can be achieved for the singlet-triplet transition than the singlet-singlet transition.

2.4 A Heat Pipe Oven as an Atomic Vapour Source

A heat pipe is used to provide a sample of Zn vapour. A diagram of the heat pipe used is shown in Figure 3.1. Zn is placed in the centre of a horizontal pipe with $MgFl_2$ windows on either side through which the beam enters and exits. The centre of this horizontal pipe is enclosed in a vertical pipe. The vertical pipe contains sodium. The sodium rests at the bottom of the vertical pipe. During operation, a coil around the bottom of the vertical pipe heats the sodium causing a column of sodium vapour to rise in the vertical pipe. Once the column of sodium vapour rises past the horizontal pipe, it uniformly heats up the Zn containing horizontal pipe. The horizontal pipe is also lined by a mesh. The mesh allows the molten Zn to rise along the sides of the pipe, via capillary action, until it coats the center of the inside of the horizontal pipe. This ensures a uniform Zn vapour. Ar gas is used as a buffer gas. The Ar limits the diffusion of Zn vapour, confining the Zn vapour in the heated centre so that it does not coat the rest of the vacuum system, especially the windows. No contamination of windows by metal vapour is an advantage of this setup. Another advantage is

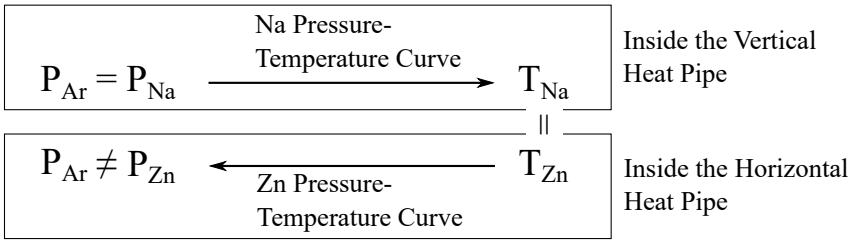

Figure 2.3: Method of indirectly measuring the temperature of the zinc, starting with measuring the pressure of the Ar buffer gas in the vertical heat pipe.

that this setup provides Zn atoms with a very homogeneous temperature and vapour pressure. In addition, the temperature is very stable - power fluctuations have no effect.

2.4.1 Pressure

To simulate the rate equations in Section 2.7, the density (Section 2.4.2) of the Zn atoms inside the heat pipe is needed. To find the density of the Zn atoms, the pressure of the Zn vapour is needed. This cannot be measured directly. However, there are two quantities that can be measured directly. The Ar buffer gas of the Zn in the horizontal section of the heat pipe can be directly measured and the Ar buffer gas of the Na in the vertical heat pipe can be measured. See Figure 3.1 for the setup of the heat pipe. The measurement of the pressure of the Ar buffer gas of the Na in the vertical heat pipe is used. After they reach thermodynamic equilibrium, the Ar and Na vapour have the same pressure. Therefore, measuring the Ar pressure will be the same as the Na vapour pressure. The temperature of Na can be found using the pressure vs temperature curve defined by the modified Antoine equation [17], Equation 2.1.

$$\log_{10}P = a + \frac{b}{T} + c\log_{10}T + \frac{d}{T^3} \tag{2.1}$$

Here, P is the pressure measured in Pa, a,b, c and d are Antoine coefficients and T is the temperature in Kelvin. The Antoine coefficients can be found from data in literature such as the Kaye and Laby Tables of Physical and Chemical Constants [4].

The horizontal section of the heat pipe is thinner than the vertical section and intersects the vertical section so that the horizontal section is surrounded by Na of a uniform temperature. Assuming that the Zn inside this horizontal section of the heat pipe is the same as the temperature of the surrounding Na vapour, the vapour pressure vs temperature curve for Zn can be used to find its pressure. A visualisation of this indirect measurement of the Zn pressure is shown in Figure 2.3.

2.4.2 Density

When the pressure and temperature of the Zn atoms are known, the density can be calculated using the Ideal Gas Law, Equation 2.2, which is a good approximation, since the Zn vapour is at a low pressure and a high temperature.

$$N = \frac{P}{k_B T} \tag{2.2}$$

where, P is the pressure in Pa, N is the number density in atoms per m^3, k_B is the Boltzmann constant, T is the temperature in Kelvin.

2.5 Velocity Distribution and Line Broadening in Vapour

2.5.1 Velocity Distribution

The Zn vapour in this experiment will have a temperature in order of 1000 K. At this high temperature, Doppler broadening has to be taken into consideration. Doppler broadening is the effect of spectral line broadening due to atoms moving in different directions and speeds relative to the incident laser beam. Some atoms will have a positive Doppler Shift, some will have a negative Doppler Shift and some will have no shift, depending on the projection of the atom's velocity in the direction of the laser beam. This results in a broadening of the spectral line observed.

Figure 2.4 shows a photon incident on a gas cell. Each atom is moving in its own direction and at its own velocity. Only the velocity in the direction of the laser, the x-direction, is important. A velocity profile is essential in the derivation of the new width of the Doppler broadened spectral line. The gas is assumed to be in thermodynamic equilibrium. The velocity distribution is then described by Maxwell-Boltzmann statistics [18].

For a certain atom, each microstate of the atom is equally likely. Consider an atom connected to a reservoir having two microstates s_1 and s_2. The probability of the atom being in state s_1 is proportional to the multiplicity of the state s_1 for the reservoir and the probability of the atom being in state s_2 is proportional to the multiplicity of state s_2 for the reservoir. This gives rise to Equation 2.3.

$$\frac{P_{s_1}}{P_{s_2}} = \frac{\Omega_R(s_1)}{\Omega_R(s_2)} \tag{2.3}$$

Here, P_{s_1} and P_{s_2} are the probabilities of the atom being in state s_1 and state s_2 respectively. $\Omega_R(s_1)$ and $\Omega_R(s_2)$ are the multiplicities of the reservoir for the states s_1 and s_2 respectively. The dependency on the multiplicity of the reservoir can be replaced by entropy, using the definition of entropy in Equation 2.4.

$$S = k_B \ln \Omega \tag{2.4}$$

Here, S is entropy, k_B is the Boltzmann constant and Ω is the multiplicity. Now, the ratio of probabilities becomes:

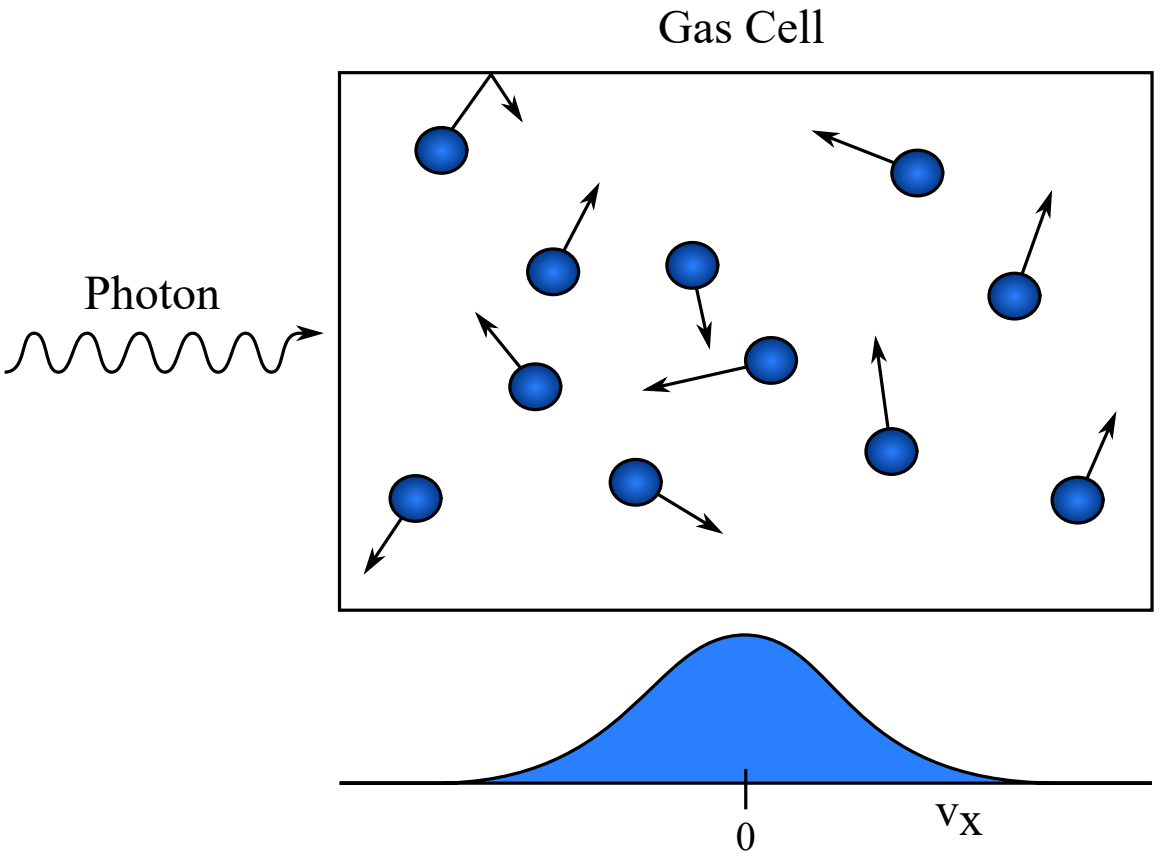

Figure 2.4: A photon is incident on a gas cell. Beneath the gas cell is the velocity distribution of the atoms in the direction of the photon, the x-direction.

$$\frac{P_{s1}}{P_{s2}} = e^{(S_R(s_1) - S_R(s_2))/k_B}. \tag{2.5}$$

Now, the thermodynamic identity given in Equation 2.6 can be invoked.

$$\mathrm{d}S = \frac{1}{T}(\mathrm{d}U + P\mathrm{d}V - \mu\mathrm{d}N) \tag{2.6}$$

where, $\mathrm{d}S$ is the change in entropy, T is the temperature, $\mathrm{d}U$ is the change in energy, $P\mathrm{d}V$ is the term related to the change in volume and $\mu\mathrm{d}N$ is the term related to the change in number of particles. As for the reservoir, it is assumed to be large enough so that $\mathrm{d}V_R$ is negligible, i.e. $PdV_R = 0$. Furthermore, the system is considered a closed system. Therefore, there is no change in the number of atoms, i.e. $\mu dN_R = 0$.

Now, the ratio of probabilities becomes

$$\frac{P_{s_1}}{P_{s_2}} = e^{(U_R(s_1) - U_R(s_2))/Tk_B}. \tag{2.7}$$

Now, using conservation of energy,

$$\frac{P_{s_1}}{P_{s_2}} = e^{(E(s_2)-E(s_1))/Tk_B}, \tag{2.8}$$

where, $E(s_1)$ and $E(s_2)$ are the energies of the atom for state s_1 and s_2. Now, the equation can be rearranged with the s_1 terms on one side and the s_2 terms on the other side. This means that s_1 and s_2 are independent and Equation 2.9 is valid for any state.

$$P_s = \frac{1}{Z} e^{-E(s)/Tk_B} \tag{2.9}$$

Z is the partition function and, here, can be viewed as a normalisation constant. Using Equation 2.9 and an energy of $\frac{1}{2}\mathrm{mv}^2$, a velocity probability distribution can be constructed for an atom moving in one direction (x-direction) and is shown in Equation 2.10.

$$P(v_x) = \left(\frac{m}{2\pi k_B T}\right)^{\frac{1}{2}} e^{-\frac{mv_x^2}{2Tk_B}} \tag{2.10}$$

The term in the square root is for normalisation. Equation 2.10 is the Maxwell-Boltzmann probability distribution function for the x-component of the velocity of atoms at thermal equilibrium.

2.5.2 Doppler Broadening

Using the Maxwell-Botzmann propability distribution function and Doppler theory, the probability distribution in frequency for the Doppler broadened transition line can be constructed. Doppler theory states that the observed frequency is higher than the source frequency by $\frac{v}{c}$ of the source frequency if the observer is moving at a velocity, v, towards the source. Equation 2.11 shows the non-relativistic Doppler shifted frequency, ν, that is observed if the observer is moving at a velocity, v, towards a source that has a frequency of ν_0.

$$\nu = \nu_0 \left(1 + \frac{v}{c}\right) \tag{2.11}$$

Solving for v the following relation is found:

$$v = \frac{c}{\nu_0} \left(\nu + \nu_0\right). \tag{2.12}$$

Now, substituting v from Equation 2.12 into the velocity probability distribution, Equation 2.10, and converting from frequency to angular frequency, the angular frequency dependent probability distribution for the Doppler broadened transition line, $s(\omega)$, is found and shown in Equation 2.13.

$$s(\omega) = \frac{c}{\omega_0}\sqrt{\frac{m}{2\pi k_B T}}e^{\frac{-m(\frac{c}{\omega_0}(\omega-\omega_0))^2}{2k_B T}} \tag{2.13}$$

The application of $s(\omega)$ to the current project is in Section 4.3.2.

2.5.3 Collision Broadening

There are other broadening effects that occur besides Doppler broadening. One such broadening mechanism is collision broadening. Collisional broadening occurs at high pressure, when the lifetime of the atoms are of the same order as the average collision times or greater. Then, atoms could collide before emitting photons, causing uncertainty of the energy of the emitted photons, increasing the spectral line width of the observed transition. Collision broadening can be investigated using Monte Carlo simulations like in the paper by Aksamija, Z [19], but this is out of the scope of this project.

2.6 Frequency Doubling and Laser Beam Propagation

The angular frequency dependent energy density profile of the laser beam, $\rho(\omega)$, is needed in the rate equation calculations. The profile is described by a Gaussian and as such, there are three values that need to be found: the central frequency, the maximum energy density for the central frequency and the bandwidth. The central frequency of the pulse that the laser is emitting is known. The beam goes through Second Harmonic Generation (SHG) directly after the laser. Therefore, the frequency is doubled. This is the central frequency of the pulse that reaches the sample.

2.6.1 Second Harmonic Generation (SHG)

The frequency bandwidth of the dye laser used is known and is shown in the resluts section (see Section 4.3.3). The bandwidth of the pulse after SHG, however, is not known and must be calculated. In order to do this a relationship between the intensity of the laser beam before and after SHG is to be derived.

Consider a plane wave with a complex amplitude, $E_j(z)$, defined by a slowly varying amplitude, $A_j(z)$, as $E_j(z) = A_j(z)e^{ik_j z}$, where z is the propagation distance and $k_j = n_j\omega_j/c$. Here, k_j is the wave number, n_j is the index of refraction, ω_j is the angular frequency ($2\omega_1 = \omega_2$ for second harmonic generation) and c is the speed of light in a vacuum. If this plane wave is incident on a non-linear second harmonic generating crystal, then the polarisation of this electric field, $E_1(z) = A_1(z)e^{ik_1 z}$, and the second harmonic electric field, $E_2(z) = A_2(z)e^{ik_2 z}$, that is produced can be expressed by Equation 2.14 and Equation 2.15 respectively [20].

$$P_1(z) = 4\epsilon_0 d_{eff} A_2(z) A_1(z)^* e^{i(k_2-k_1)z} \tag{2.14}$$
$$P_2(z) = 2\epsilon_0 d_{eff} A_1(z)^2 e^{2ik_1 z} \tag{2.15}$$

where, ϵ_0 is the permittivity of free space, and d_{eff} is the effective nonlinear optical coefficient. Applying the driven wave equation, the coupled differential equations for the slowly varying amplitude of the seed electric field, $A_1(z)$, and the slowly varying amplitude of the second harmonic electric field, $A_2(z)$ is shown in Equation 2.16 [20].

$$\begin{aligned}\frac{\mathrm{d}}{\mathrm{d}z}A_1(z) &= \frac{2i\omega_1^2 d_{eff}}{k_1 c^2} A_2(z) A_1(z)^* e^{-i\Delta k z} \\ \frac{\mathrm{d}}{\mathrm{d}z}A_2(z) &= \frac{i\omega_2^2 d_{eff}}{k_2 c^2} A_1(z)^2 e^{i\Delta k z}\end{aligned} \tag{2.16}$$

Here, $\Delta k = 2k_1 - k_2$.

The relationship between the slowly varying field amplitude and its corresponding intensity, $I_j(z)$, is shown in Equation 2.17 [20].

$$I_j(z) = 2n_j\epsilon_0 c|A_j|^2 \tag{2.17}$$

Using Equation 2.17, the Manley-Rowe relations (which results in the total intensity, $I = I_1 + I_2$, being invariant under propagation) and assuming that the incident light is not depleted, i.e. $A_1(z)$ is constant, the differential equation for the second harmonic field shown in Equation 2.16 can be integrated [20] to find the intensity of the second harmonic beam after travelling a distance, l, through a second harmonic generating material such as a BBO (β-Barium Borate) crystal. The resulting relation is a sinc function as displayed in Equation 2.18.

$$I_2(l) = \left(\frac{i\omega_2 d_{eff} l}{n_1 c}\right)^2 \left(\frac{1}{2n_2\epsilon_0 c}\right) \left(\frac{\sin(\frac{1}{2}\Delta k l)}{\frac{1}{2}\Delta k l}\right)^2 I_1(l)^2 \tag{2.18}$$

This shows that the intensity of the second harmonic pulse is proportional to the square of the intensity of the pulse before SHG. Using this and the general formula for a Gaussian that is used to approximate the pulses, the FWHM of the pulse, going through SHG, decreases by a factor $\sqrt{2}$. However, due to the doubling of the frequency, the FWHM also doubles. The net change in the FWHM is an increase by a factor $\sqrt{2}$.

The reason why phase matching is important can be seen in Equation 2.18. The maximum second harmonic intensity is achieved with the phase matched condition $\Delta k = 0$. The phase matched condition is met in the experiment by rotating the nonlinear crystal to a specific angle for each wavelength of the output of the laser. Figure 2.5 illustrates different types of phase matching and the relative polarisation directions of the electric fields of the fundamental (ω) and the second harmonic (2ω) waves. BBO is a negative

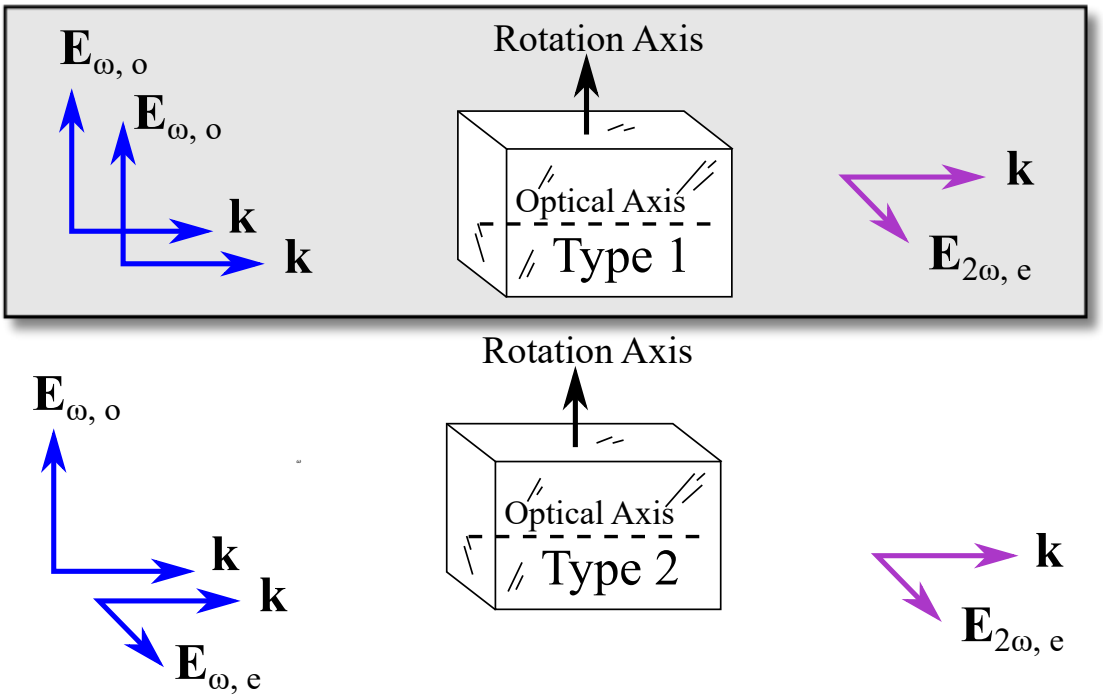

Figure 2.5: Types of phase matching for SHG for a negative uniaxial crystal, where, ω is the angular frequency of the pulse. o and e indicate the ordinary and extra-ordinary waves respectively. **k** is the propagation vector and the orientations of the linearly polarised electric fields are shown as arrows.

uniaxial crystal (ordinary index of refraction, $n_o >$ extra-ordinary index of refraction, n_e) and type 1 phase matching is used in the current setup. Therefore, the second harmonic electric field is polarised horizontally, perpendicular to the vertically polarised fundamental electric field. The crystal is rotated around the vertical axis (See Figure 2.5) to achieve phase matching at a particular fundamental wavelength.

The calibration that is needed to synchronise the crystal rotation with the wavelength scanning can be seen in Section 4.2.

2.6.2 Fresnel Equations

The maximum energy density for the central frequency can be found if the intensity of the pulse is known. The energy meter used can measure the energy of the laser beam before SHG, but does not have the sensitivity to measure the energy of the pulse after SHG, so an approximation of the intensity of the pulse at the heat pipe is calculated. To find the intensity of the laser pulse that reaches the sample, the laser intensity is measured after the dye laser and then the transmittance of each optic before the sample is calculated to find the intensity of the beam just before the sample.

The results for BBO efficiency from Rahman, A. 2018 [21] are used to find the efficiency of the BBO crystal that is used.

The BBO crystal used is cut for Type 1 phase matching. Therefore, a horizontally polarised second harmonic pulse is generated from the vertically polarised laser pulse incident on it. After SHG the optics ($MgFl_2$ windows, UV-coated Al mirrors and UV-grade fused Si Prisms) used to direct and manipulate the pulse are arranged on a horizontal plane, the same plane as the polarisation plane of the second harmonic pulse. This means that the pulse is p-polarised.

Fresnel Equations are used to find the transmittance, T, for the optics used. The Fresnel Equations for p-polarised light [14] is seen in Equation 2.19.

$$T_{||} = \left(\frac{n_t \cos\theta_t}{n_i \cos\theta_i}\right)\left(\frac{2n_i \cos\theta_i}{n_i \cos\theta_t + n_t \cos\theta_i}\right)^2 \tag{2.19}$$

where, θ_i is the incident angle, θ_t is the transmitted angle, n_i is the refractive index of the first material, θ_t is the refractive index of the second material and $T_{||}$ is the transmittance for p-polarised light.

2.7 Rate Equation model

An Einstein rate equation model of a two-state system is used to simulate the experiment. This is valid, because, for the $4s^2\ {}^1S_0 \rightarrow 4s4p\ {}^1P_1{}^o$ transition, the excited state only has the ground state to decay to. Three processes are possible in a typical two-state system:

1. **Spontaneous emission** from the excited state to the ground state.
2. **Stimulated emission** from the excited state to the ground state.
3. **Absorption** from the ground state to the excited state

These three processes form the three terms in the rate equation model describing the population density in both states as shown in Equations 2.20 [22].

$$\begin{aligned}
\frac{\mathrm{d}N_1}{\mathrm{d}t} &= \overbrace{A_{21}N_2}^{\text{Spontaneous Emission}} + \overbrace{B_{21}N_2\int_0^\infty \rho(\omega)s(\omega)\mathrm{d}\omega}^{\text{Stimulated Emission}} - \overbrace{B_{12}N_1\int_0^\infty \rho(\omega)s(\omega)\mathrm{d}\omega}^{\text{Absorption}} \\
\frac{\mathrm{d}N_2}{\mathrm{d}t} &= -A_{21}N_2 - B_{21}N_2\int_0^\infty \rho(\omega)s(\omega)\mathrm{d}\omega + B_{12}N_1\int_0^\infty \rho(\omega)s(\omega)\mathrm{d}\omega
\end{aligned} \tag{2.20}$$

Here, N_1 and N_2 are the population number density of the ground state and excited state respectively. $\rho(\omega)$ is the power density profile of the incident laser pulse. $s(\omega)$ is the transition profile of the transition between the ground state and the excited state. The first, second and third term relates to spontaneous emission, stimulated emission

and absorption respectively. The sign of each term indicates whether that term increases or decreases N_1 and N_2. Assuming an ideal two state atom, the atoms that are not in the excited state must be in the ground state, i.e. $N = N_1 + N_2$, where N is the total number density. So the rate equation for the ground state is just the negative of the equation for the excited state as seen in Equations 2.20.

2.7.1 Degeneracy and relationship between Einstein Coefficients

The Einstein rate equation model takes degeneracy into account by relating B_{12} and B_{21} using Equation 2.21 [22].

$$B_{12} = \frac{g_2}{g_1} B_{21} \tag{2.21}$$

where, B_{12} is the Einstein B coefficient for stimulated absorption, B_{21} is the Einstein B coefficient for stimulated emission, g_1 is the degeneracy of the ground state and g_2 is the degeneracy of the excited state. For the transition, $4s^2\ {}^1S_0 \rightarrow 4s4p\ {}^1P_1{}^o$, the excited state is three-fold degenerate due to it having J=1 $\rightarrow$ m_j = 0, 1, 2. Therefore, there exists essentially one ground state and three excited states with the same energy and each excited state can only decay into the ground state.

The relationship between the A and B coefficients are needed in order to find the values for the B coefficients if only the A coefficients are given in literature, which is often the case. The relationship between the A and B coefficients are given by 2.20 [22],

$$B_{21} = \frac{A_{21}\lambda^3}{8\pi\hbar}. \tag{2.22}$$

2.8 Absorption Cross-Section

Consider the case of photons that are incident on a sample, not unlike inside the heat pipe, where the laser is incident on zinc gas. Not all the photons will interact with the sample, some will interact with the sample, the rest will move through the sample without interacting. The absorption cross-section is a measure of how likely it is for the photons to interact with atoms or molecules in this sample. The absorption cross section is different from the actual physical space that the atom occupies, because it is frequency dependent. The closer the photons are to resonance the bigger the absorption cross-section will be.

There are three possible ways to find the absorption cross-section. The first is to assume that the laser bandwidth, $\rho(\omega)$, is much narrower than the transition width, $s(\omega)$, i.e. $\rho(\omega) << s(\omega)$. Thus, $s(\omega)$ is constant in the region of the laser bandwidth. This is called the **Narrowband Approximation**. The second is to assume that the laser bandwidth, $\rho(\omega)$, is much broader than the transition width, $s(\omega)$, i.e. $\rho(\omega) >>$

$s(\omega)$. Thus, $\rho(\omega)$ is constant in the region of the laser bandwidth. This is called the **Broadband Approximation**. The final way is to use the Einstein rate equations without making use of either of the previous two approximations. This will be referred to as the **General Relation**.

2.8.1 General Relation

The absorption cross-section multiplied by the photon flux determines the rate of both the stimulated emission and the stimulated absorption. The absorption cross-section, $\sigma(\omega)$, is defined (for the two-state atom model) by the relation,

$$\frac{\mathrm{d}N_2}{\mathrm{d}t} = -A_{21}N_2 - \frac{\sigma(\omega)I}{\hbar\omega}\left[N_2 + \frac{g_2}{g_1}N_1\right]. \tag{2.23}$$

$\frac{\sigma(\omega)I}{\hbar\omega}$ is the total photon flux, where the total intensity, I, is related to the total energy density, ρ, by

$$I = \int_{-\infty}^{\infty} I(\omega)\mathrm{d}\omega = c\int_{-\infty}^{\infty}\rho(\omega)\mathrm{d}\omega = c\rho. \tag{2.24}$$

Comparing equation 2.23 to the Einstein rate equation as seen in Equation 2.20 yields the general relation for the absorption cross-section:

$$\sigma(\omega) = \frac{B_{21}\hbar\omega}{I}\int_{-\infty}^{\infty}\rho(\omega)s(\omega)\mathrm{d}\omega \tag{2.25}$$

Applying the relation between B_{21} and A_{21} (Equation 2.22) yields,

$$\sigma(\omega) = A_{21}\frac{c\lambda^2}{4I}\int_{-\infty}^{\infty}\rho(\omega)s(\omega)\mathrm{d}\omega \tag{2.26}$$

2.8.2 Narrowband Approximation

In the narrowband approximation, $s(\omega)$ is assumed to be constant. Therefore,

$$\int_{-\infty}^{\infty}\rho(\omega')s(\omega')\mathrm{d}\omega' = s(\omega)\int_{-\infty}^{\infty}\rho(\omega')\mathrm{d}\omega' = s(\omega)\rho. \tag{2.27}$$

Using the general relation for the absorption cross-section (Equation 2.26) and the relationship between the Einstein A and B coefficients (Equation 2.22), the absorption cross-section for the narrowband approximation is found to be

$$\sigma(\omega) = A_{21}\frac{\lambda^2}{4}s(\omega). \tag{2.28}$$

An estimation of the absorption in the heat pipe, for the central frequency, is calculated and tabulated in Table 4.4 using both the narrowband and general relation.

2.8.3 Broadband Approximation

For the broadband approximation, $\rho(\omega)$ is assumed to be constant. Therefore,

$$\int_{-\infty}^{\infty} \rho(\omega')s(\omega')\mathrm{d}\omega' = \rho(\omega)\int_{-\infty}^{\infty} s(\omega')\mathrm{d}\omega' = \rho(\omega)s. \tag{2.29}$$

Similar to the narrowband approximation, the absorption cross-section for the broadband approximation can be calculated using the general relation for the absorption cross-section (Equation 2.26), the relationship between the Einstein A and B coefficients (Equation 2.22) as well as the relationship between I and ρ (Equation 2.24). The absorption cross-section for the broadband approximation is found to be

$$\sigma(\omega) = A_{21}\frac{\lambda^2 I(\omega)}{4I} \tag{2.30}$$

where a distinction needs to be made between $I(\omega)$ and I. $I(\omega)$ is the angular frequency dependent intensity, where I is the intensity integrated over all frequencies.

The broadband approximation is not applicable to simulate the current experiment, and is not used.

2.9 Calculating Absorption in a Sample Using the Rate Equations

Absorption in a sample at low light intensities is described by the Beer-Lambert law. This law assumes that the transfer of population to the excited state and the rate of the stimulated emission are both negligible. Therefore, the absorption cross-section, σ and the absorption coefficient, $\alpha(\omega) = \sigma(\omega)N$ are both independent of the light intensity and constant throughout the beam path. In this case,

$$\frac{\mathrm{d}I(z)}{\mathrm{d}z} = -\alpha(\omega)I(z) \tag{2.31}$$

is integrated to yield,

$$I(z) = I(0)e^{-\alpha z} \tag{2.32}$$

In our experiment, the transition is easily saturated. Significant population is transferred to the excited state so that the assumptions of the Beer-Lambert Law are not valid.

Instead of using $\alpha(\omega) = \sigma(\omega)N$, as in the Beer Lambert Law, in the rate equations, the rate at which photons are being absorbed by the medium is used to define the absorption coefficient, $\alpha(\omega)$, as seen in Equation 2.33 [22].

$$\alpha(\omega) = -\sigma(\omega)\left(N_2 - \frac{g_2}{g_1}N_1\right) \tag{2.33}$$

Applying the steady state condition, $\mathrm{d}N_2/\mathrm{d}t = 0$, and $N = N_1 + N_2$, results in [22],

$$\alpha(\omega) = \left(\frac{g_2}{g_1}\right)\frac{\sigma(\omega)N}{1 + \left(1 + \frac{g_2}{g_1}\right)\frac{\sigma(\omega)I}{\hbar\omega A_{21}}}. \tag{2.34}$$

Defining the saturation intensity as [22],

$$I_{sat} = \frac{\hbar\omega A_{21}}{\sigma(\omega)}, \tag{2.35}$$

results in the final form of the absorption coefficient,

$$\alpha(\omega) = \left(\frac{g_2}{g_1}\right)\frac{\sigma(\omega)N}{1 + \left(1 + \frac{g_2}{g_1}\right)\frac{I}{I_{sat}}} \tag{2.36}$$

To find the relationship between the intensity of the beam after a length z, $I(z)$, the initial intensity, $I(0)$ and the temperature, T, the differential equation, Equation 2.31, is used. All variables that depend on $I(z)$, $I(0)$ and T need to be substituted, this includes, $\alpha(\omega)$, which depends on $\sigma(\omega)$, N, $I(z)$ and I_{sat}. $\sigma(\omega)$, for which the narrowband approximation will be used (Equation 2.28), depends on $s(\omega)$, which depends on T (See Equation 2.13). N depends on T. I_{sat} depends on $\sigma(\omega)$ and, therefore, T. These dependencies are indicated in Equation 2.37, derived by the author.

$$\frac{\mathrm{d}I(z, I(0), T)}{\mathrm{d}z} = -\left(\frac{g_2}{g_1}\right)\frac{A_{21}\frac{\lambda^2}{4}s(\omega, T)N(T)}{1 + \left(1 + \frac{g_2}{g_1}\right)\frac{I(z,I(0),T)}{I_{sat}(I(0),T)}}I(z, I(0), T) \tag{2.37}$$

Equation 2.37 can be solved numerically using Mathematica. For a propagation length $z = 0.06$ m, the fraction of absorption, $f_{abs} = (I(0) - I(z, I(0), T))/I(0)$, is plotted versus temperature and initial intensity in Figure 4.15.

In a similar manner, the dependencies on the wavelength, λ, can be traced and is shown in Equation 2.38.

$$\frac{\mathrm{d}I(z, \lambda)}{\mathrm{d}z} = -\left(\frac{g_2}{g_1}\right)\frac{A_{21}\frac{\lambda^2}{4}s(\lambda)N}{1 + \left(1 + \frac{g_2}{g_1}\right)\frac{I(z,\lambda)}{I_{sat}}}I(z, \lambda) \tag{2.38}$$

Equation 2.38 can be solved numerically using Mathematica. For the current experimental conditions, the fraction of absorption, $f_{abs} = (I(0) - I(z, \lambda))/I(0)$, is plotted versus wavelength in Figure 4.21.

2.10 Saturation Intensity

A distinction between the saturation intensity, I_{sat}, and the intensity that is needed to saturate a transition needs to be made. I_{sat} defined in Equation 2.36 is the intensity where significant population transfer to the upper state starts to occur. For Equation 2.36, when $g_2 = g_1$, I_{sat} is the intensity that causes the absorption coefficient to become half of the value that it would have been if, instead, the intensity approached zero. The intensity that is needed to saturate a transition, on the other hand, is larger and represents the intensity, where the population in the upper state is close to the highest possible population.

Using the rate equations at steady state, i.e. $\mathrm{d}N_2/\mathrm{d}t = 0$, and assuming spontaneous emission is much less frequent than stimulated emission and absorption, the relation between the populations in the lower and upper state is as follows:

$$N_2 = \frac{g_2}{g_1} N_1. \tag{2.39}$$

Here, N_2 and N_1 are the populations in the upper and lower states respectively and g_2 and g_1 are the degeneracies of the upper and lower states respectively. Assuming a closed two-atom system, i.e. $N_1 + N_2 = N$, Equation 2.39 becomes:

$$N_2 = \frac{g_2/g_1}{1 + g_2/g_1} N. \tag{2.40}$$

For the $4s^2\ {}^1S_0 \rightarrow 4s4p\ {}^1P_1{}^o$ transition, $g_2 = 3$ and $g_1 = 1$. This results in the maximum fraction of the total atom density, N, that the upper population, N_2, can reach:

$$N_2 = \frac{3}{4} N. \tag{2.41}$$

The intensities needed to approach these values for N_2 are explored in simulations in Section 4.4 for the $4s^2\ {}^1S_0 \rightarrow 4s4p\ {}^1P_1{}^o$ transition as well as the $4s^2\ {}^1S_0 \rightarrow 4s4p\ {}^3P_1{}^o$ transition, which has the same degeneracies.

3. Experimental Setup

In order to study the absorption spectrum of Zn using a heat pipe, there are certain essential components needed, as listed below:

1. **Heat Pipe:** This will be used as a source as well as housing for the Zn vapour.
2. **Lasers:** These will be used to excite the Zn atoms along specific transitions.
3. **Second Harmonic Generation (SHG):** SHG is needed to produce the correct wavelength pulses.
4. **Detection and Data Processing:** A Si detector, an oscilloscope and Python program will be used to detect and process the data.

These components and their uses will be described in the following sections.

3.1 Heat Pipe

Section 2.4 describes the details of the heat pipe. For this experiment, a heat pipe was chosen as the source of Zn instead of a gas cell or a Hollow Cathode Lamp (HCL). The reason why a gas cell can't be used is simply because Zn is a solid at room temperature. The reason why a heat pipe is superior to a HCL for this experiment is because the heat pipe produces Zn vapour with a known length and a calculable density. Therefore, we can calculate the absorption cross section from an absorption measurement in the heat pipe.

The typical Ar pressure for the vertical pipe, P_1, is 75 kPa and the typical pressure of the horizontal pipe, P_2, is 76 kPa. A heating coil is used to heat up the Na in the vertical pipe. A heating power of 800 W is used. Two type K thermocouples are used to make sure that the Na vapour column is at the right height - not too low as to not completely cover the horizontal pipe and not too high as to seep into the rest of the vacuum system (See positioning in Figure 3.1). After equilibrium is reached, the temperature of the bottom thermocouple reaches 1100 K and the top thermocouple reaches 800 K. The vapourisation of Zn causes a small increase in the pressure of the system, but it is small due to the large volume of the Ar resevoir. At equilibrium the pressure of the system is stable

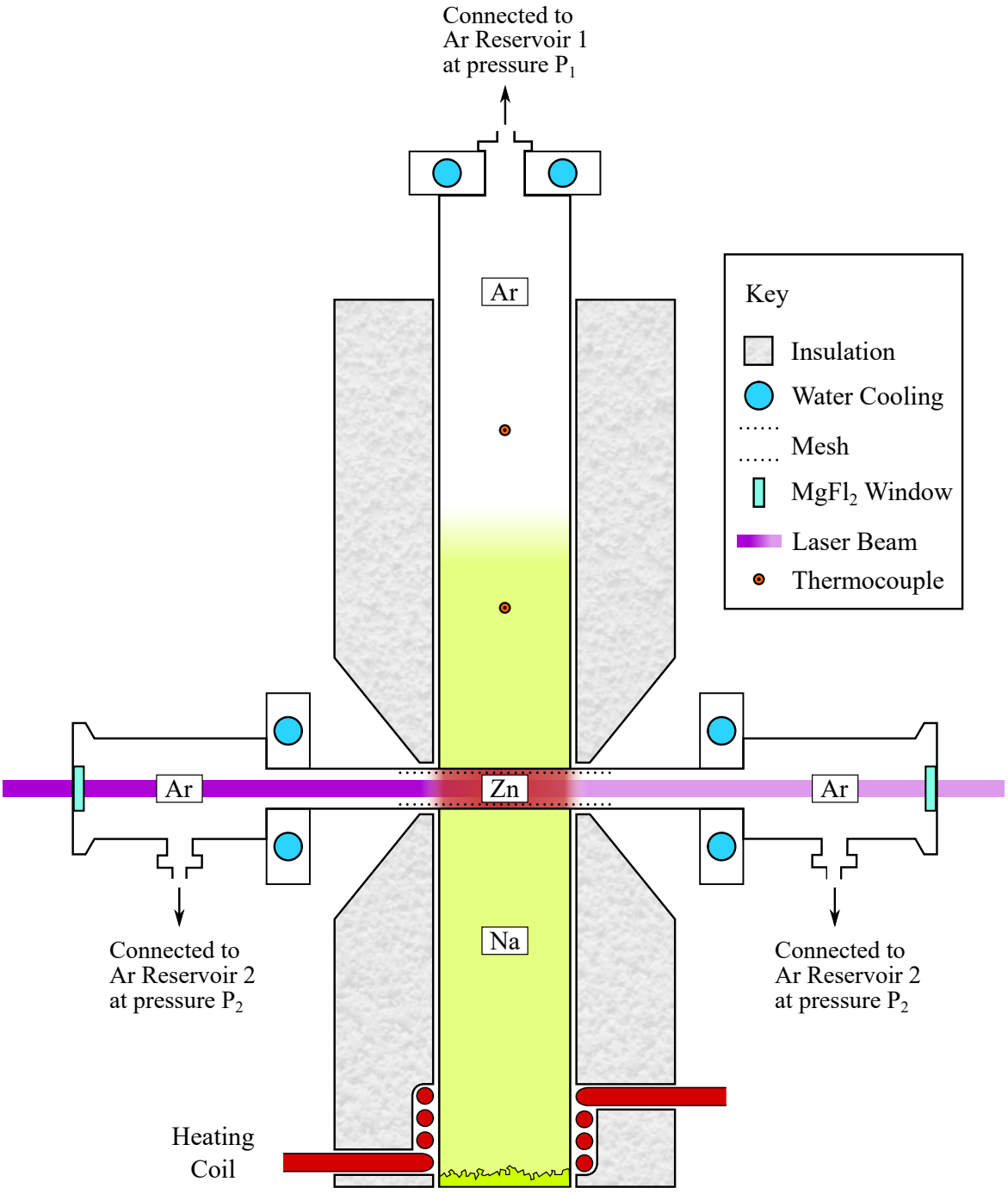

Figure 3.1: Diagram of the heat Pipe.

3.2 Lasers and Calibration

A Lambda Physik dye laser is used. It is pumped by a Nd:YAG laser that produces pulses with a wavelength of 355 nm, a spot-size of 2 mm and a temporal width of 8 ns. Stilbene 3 (Stilbene 420) dye from Radiant Dyes is used as the dye for the Lambda Physik laser. The concentration for the dye is 0.22 gram/L and the solvent used is 70% ethanol and 30% distilled water. The tuning range of Stilbene 3 is between 415 nm and 450 nm with maximum output at 430 nm. Stilbene 3 has an efficiency of 13% for the needed 428 nm [23].

Once the dye is replaced and the laser is aligned, it needs calibration. For calibration, a see-through Zn Hollow Cathode Lamp (HCL) is used. It contains Neon as a buffer gas. Neon has transition lines in the wavelength region of interest and the measured peaks can be compared to the known lines from the Atlas of Optogalvanic Transitions in Neon [3] which were also measured in a HCL. The lamp current is displayed on a digital oscilloscope and measurement is done by gated integration over a part of the signal.

The calibration results are presented in Section 4.1.

3.3 Second Harmonic Generation and Calibration

Second Harmonic Generation (SHG) is used to produce pulses with a wavelength of 214 nm in order to stimulate the ground state $4s^2\ ^1S_0$ to excited state $4s4p\ ^1P_1{}^o$ transition. A β-Barium Borate (BBO) crystal is used to achieve SHG and a compensator is used to compensate for beam deviation. Figure 3.2 shows a diagram of the setup that is used for SHG. The setup is from Radiant Dyes. A stepper motor controls the movement of the BBO crystal and the compensator. The motor ensures that the BBO crystal and the compensator rotate by the same angle but in opposite directions as indicated in Figure 3.2. This ensures that when different wavelengths are scanned, the outgoing beam stays on the same path. A stepper motor driver (Synertronic Designs, Uragan) and a custom Labview program written by Andre De Bruyn (PhD student) is used to drive the motor.

The angular orientation of the BBO crystal has to be matched to the incident wavelength and change correctly as the laser wavelength is tuned (see Section 2.6). This phase matching requirement is fulfilled by calibrating the SHG setup. By calibrating the crystal orientation versus the dye laser wavelength, efficient SHG is achieved. However, calibration cannot be performed without beam separation. Currently, two-prism beam separation is used to isolate the second harmonic beam (See "Beam Separation" in Figure 3.3).

The SHG was calibrated in the past, so the stepper motor steps are already converted to wavelengths in the Labview program, but now that the dye in the Lambda Physik laser has been changed and the laser has been re-calibrated, the wavelengths associated with the SHG need to be re-calibrated. To calibrate the SHG setup, the calibrated dye

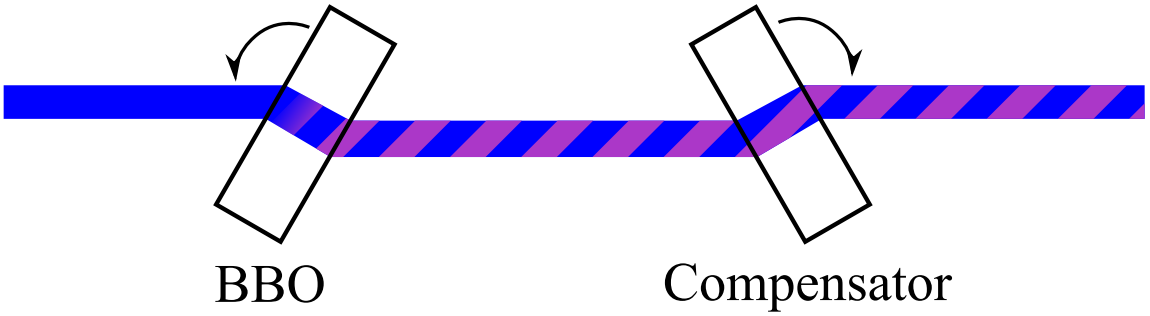

Figure 3.2: Second Harmonic Generation Setup.

laser is used in the step-by-step process outlined below.

- **Step 1: Set Dye Laser.** First the dye laser is set to a certain wavelength close to the operating wavelength.
- **Step 2: Scan the SHG System.** Scanning the orientation of the BBO and compensator crystals produces a phase matching curve as can be seen in Figure 4.3. The phase matching curve is recorded using a Si detector from Thorlabs (DET10A).
- **Step 3: Repeat Step 1-2.** Find the phase matching curve for different wavelengths in the region that you want the SHG to be calibrated in.
- **Step 4: Find the centre of the peaks.** Find the central wavelength of each phase matching peak by fitting a Gaussian to each peak. These central wavelengths are supposed to be the same as half the wavelength of the laser, but since the system is not calibrated yet, it will not be exactly the same.
- **Step 5: Compare the wavelengths.** For each scan, plot the central wavelength of the peak vs half of the wavelength of the Lambda Physik dye laser and fit a line through it.
- **Step 6: Input conversion into Labview program.** Use the fitted line to calibrate the system to ensure that the SHG crystal will automatically be rotated to the correct angle during wavelength scanning of the dye laser.

Typical calibration results are presented in Section 4.2.

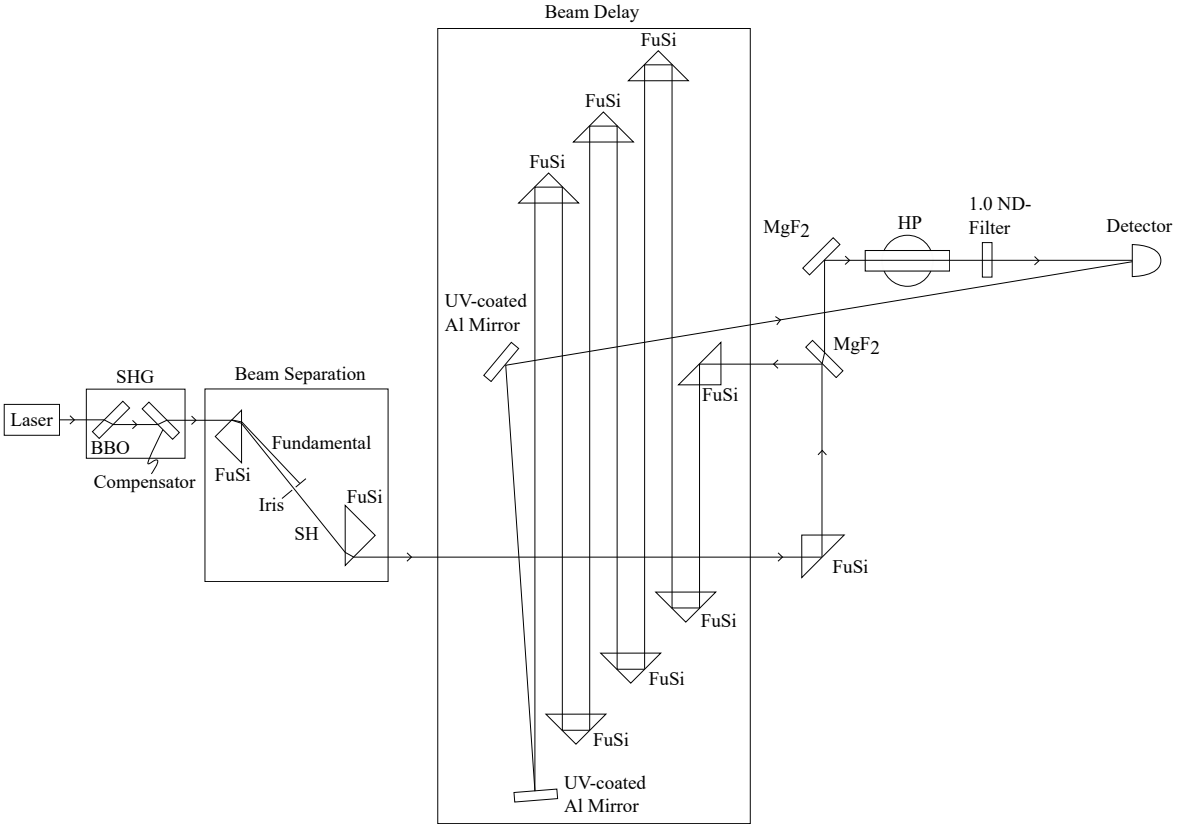

Figure 3.3: Experimental setup for Atomic Absorption Spectroscopy (AAS) of Zn inside a heat pipe, including Second Harmonic Generation (SHG), beam separation, beam delay and detection.

3.4 Atomic Absorption Spectroscopy Setup

Figure 3.3 shows the experimental setup for Atomic Absorption Spectroscopy (AAS) of Zn inside a heat pipe, including Second Harmonic Generation (SHG), beam separation, beam delay and detection. A BBO crystal is used for SHG. Two right angled UV-grade fused-silica prisms from Thorlabs are used for beam separation. A MgF_2 window is used to split the reference beam from the sample beam that goes through the heat pipe (HP). A combination of fused-silica prisms and UV-coated Al mirrors delay the beam by 150ns (45 m of air). To direct the beam into the HP, a MgF_2 window is used. A ND-filter from Edmund Optics is used to decrease the intensity of the sample beam to an intensity similar to that of the delayed reference beam. To detect both beams, a Si detector from Thorlabs (DET10A) is used. This detector has a rise time of 1 ns and a detection area of 0.8 mm^2. The signal from the detector is sent to an oscilloscope (Tektronix TDS2014). The trace from the oscilloscope (average of 64 pulses) is downloaded to a computer for analysis.

3.5 Data Processing

A Python program was written to analyse the traces that are imported from the oscilloscope. Figure 3.4 shows the interface of the analysis program. The program reads in

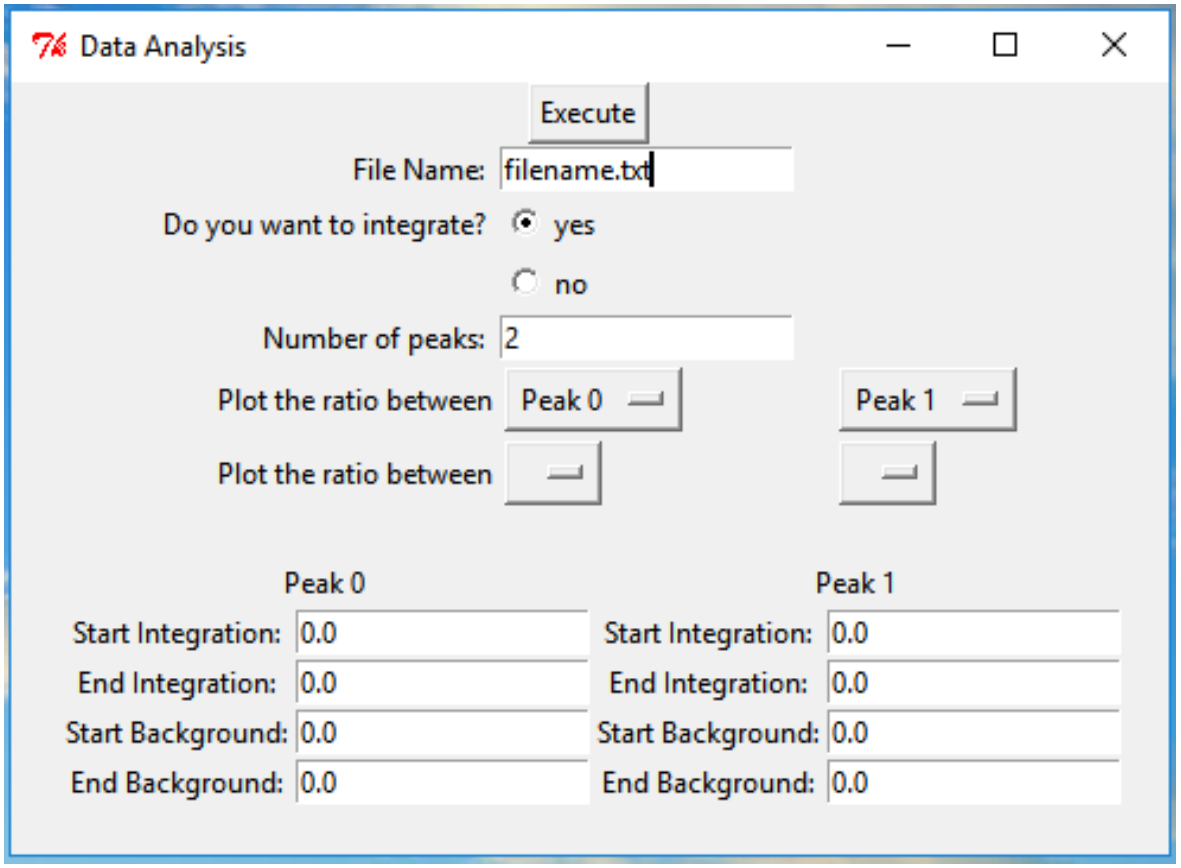

Figure 3.4: Data analysis program interface.

the traces from the Oscilloscope in a txt or csv file. It asks you if you want to integrate. If you say "no" it will just plot the traces. If you say "yes" it will integrate over the number of peaks you specify as well as show the ratio between the integrated peaks desired - which is useful when trying to find absorption. For each peak you need to specify the time interval to integrate and the time interval to consider as background. The program subtracts the background and integrates each peak using the Simpsons method.

4. Results and Discussion

4.1 Laser Calibration

Laser wavelength calibration is done, as discussed in Section 3.2, by measuring an optogalvanic spectrum of Neon lines in a Hollow Cathode Lamp (HCL), as illustrated in Figure 4.1 and Figure 4.2. Figure 4.1 shows three scans of the Lambda Physik laser before calibration as well as the calibration line produced from this data. The first two scans are done with wavelength steps of 0.02 nm and the last one is done with steps of 0.01 nm. The Gaussian fits have FWHM values of 0.02 - 0.07 nm. The differences between the central wavelength value of a particular peak in different scans is 0.0007 - 0.005 nm, which is less than the step size. Therefore, it can be concluded that the Lambda Physik dye laser wavelength has an accuracy of less than 0.01 nm. The cause of the change in wavelength could be due to a change in temperature, since the laser is not actively cooled.

To obtain the calibration curve in Figure 4.1d, the average of the data from Figures, 4.1a, 4.1b and 4.1c were used. The vertical error bars represent the error in the average . It was calculated by standard error propagation from the FWHM values of the individual Gaussian fits. The linear calibration function obtained from Figure 4.1d is given in Table 4.1.

Figure 4.2a shows an independently measured optogalvanic spectrum that was calibrated using the calibration function from Table 4.1. Figure 4.2b shows the difference between the calibrated, experimental wavelengths measured and literature values for the same transitions. The calibrated wavelengths are within 0.01 nm of the literature wavelengths, confirming that the laser wavelength readout is accurate to ± 0.01 nm.

Equation	$y = a + bx$	
Adj. R-Square	0.99998	
	Value	**Standard Error**
a	3.68166	6.36815
b	0.99493	0.01497

Table 4.1: Fitted values for the Lamdba Physik calibration fit.

The linear calibration curve is a good fit, with an adjusted R-Square value of 0.99998. The error in the a value is large because the region over which this calibration was done is narrow (1.6 nm) and far from the y-axis (425 nm). A better fit could be made with more scans.

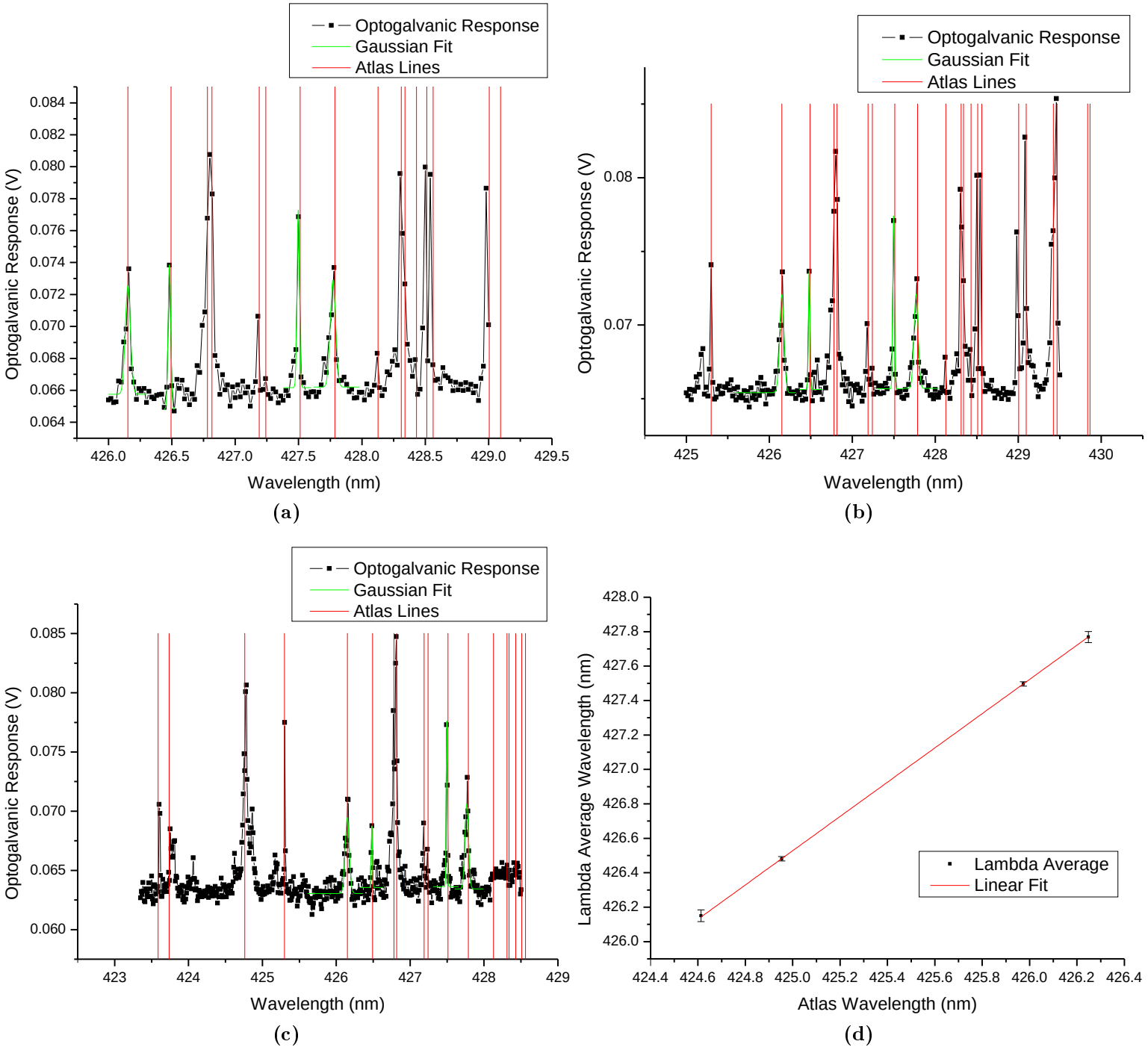

Figure 4.1: 4.1a-4.1c are scans of Neon lines used as the buffer gas inside a Zn HCL. The first two scans were done on the same day and the third one was done three days later. The vertical red lines are measured Neon lines from the Atlas of Optogalvanic Transitions in Neon [3], but shifted by 1.53871 nm so that they roughly line up with our measured peaks. The green peaks are Gaussian fits of four peaks that will be used in the calibration. The average of the central wavelength of these fits over the four scans are shown in the y-axis of Figure 4.1d. The x-axis shows the corresponding wavelength from the Atlas of Neon lines.

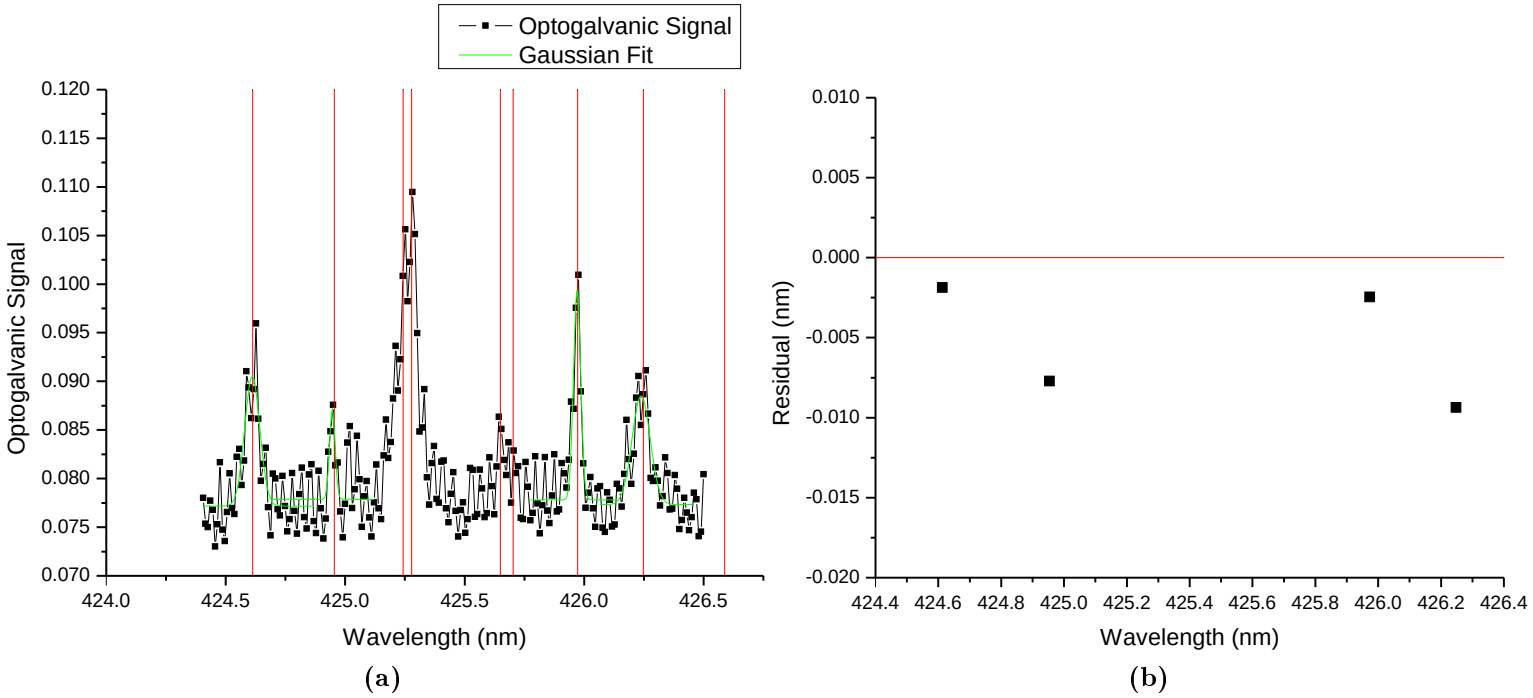

Figure 4.2: Figure 4.2a shows the optogalvanic response from the HCL with respect to wavelength after calibration. The green curves are Gaussian fits. The red lines indicate the wavelengths of known Neon lines from the Atlas of Optogalvanic Transitions in Neon [3]. Figure 4.2b shows the difference between measured wavelengths produced by our Lambda Physik laser after calibration and the known wavelengths from the Atlas [3].

4.2 Second Harmonic Generation (SHG) Phase Matching Calibration

Using the step-by-step method described in Section 3.3, the phase matching curve for 9 wavelengths were recorded in the region 427.4 nm - 428 nm (laser wavelength), generating second harmonic in the region 213.7 nm to 214 nm. Figure 4.3 shows the phase matching curve for second harmonic at 213.875 nm. The phase matching curve is described as a Sinc-function in Section 2.6.1. However, as only the centre of the main peak is relevant, a Gaussian curve was fit to the main peak to determine the centre, as shown in Figure 4.3.

Figure 4.4 shows the wavelength of the previous calibration on the y-axis (labelled as "BBO setting") and half of the wavelength of the calibrated Lambda Physic laser on the x-axis (labelled as "Wavelength of Second Harmonic"). This is the calibration used to synchronise the rotation of the crystals in the SHG unit with the wavelength of the dye laser during wavelength tuning to ensure that phase matching is maintained.

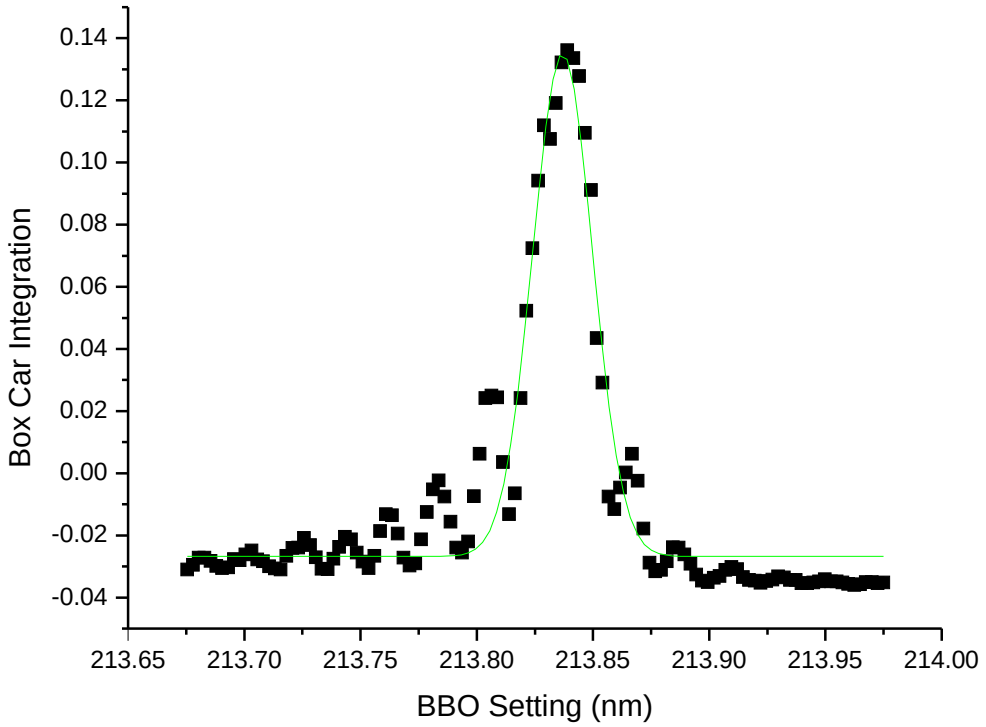

Figure 4.3: Gaussian fit of the phase matching curve for 213.875 nm, with a Gaussian function fitted to determine the centre of the main peak. The values on the horizontal axis are the setting of the BBO crystal that has to be recalibrated.

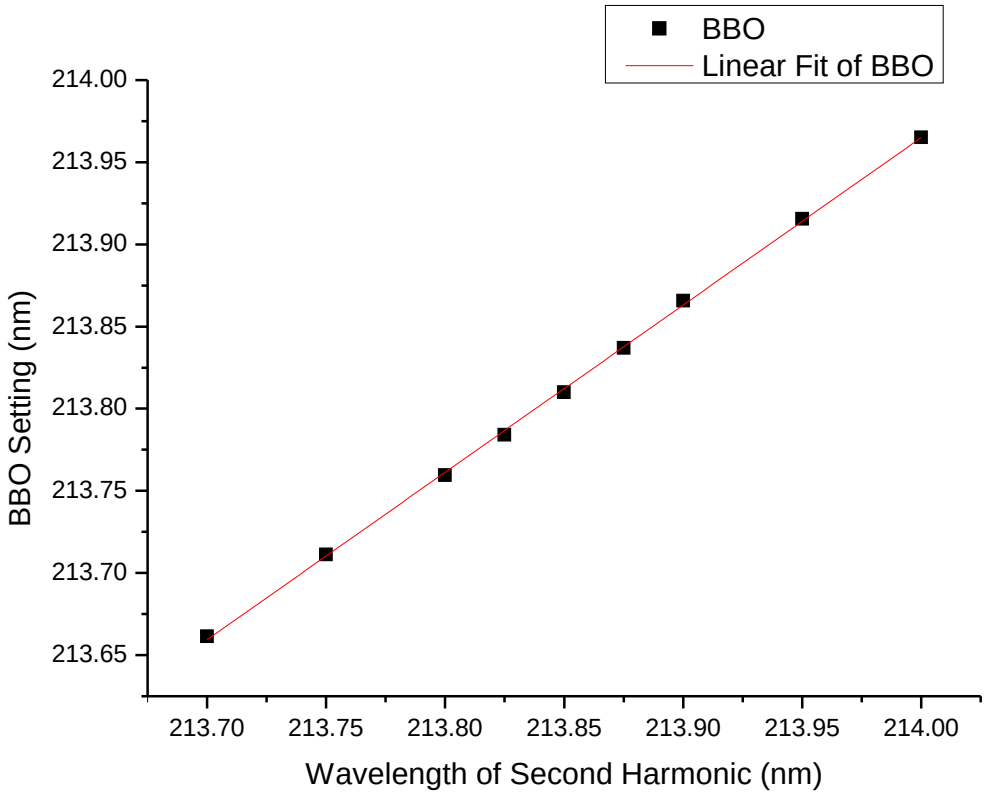

Figure 4.4: Linear fit for calibration of the BBO crystal setting to generate second harmonic at wavelengths in the range 213.7 - 214.0 nm.

4.3 Einstein Rate Equation model

The aim is to simulate the change in light intensity and populations of the energy levels of Zn atoms in the Zn vapour as applicable to the experimental setup, when the laser frequency is tuned over the resonance of the $4s^2\ {}^1S_0 \rightarrow 4s4p\ {}^1P_1{}^o$ transition of Zn.

To analyse the dynamics of populations in the sample, the Einstein rate equation model for a two state system is used. In Section 2.7, it is shown that the general rate equations for the two states are given as two coupled first-order differential equations as shown in Equation 2.20, repeated below for convenience.

$$\frac{\mathrm{d}N_1}{\mathrm{d}t} = A_{21}N_2 + B_{21}N_2\int_0^\infty \rho(\omega)s(\omega)\mathrm{d}\omega - B_{12}N_1\int_0^\infty \rho(\omega)s(\omega)\mathrm{d}\omega$$
$$\frac{\mathrm{d}N_2}{\mathrm{d}t} = -A_{21}N_2 - B_{21}N_2\int_0^\infty \rho(\omega)s(\omega)\mathrm{d}\omega + B_{12}N_1\int_0^\infty \rho(\omega)s(\omega)\mathrm{d}\omega$$

where N_1 and N_2 are the number density of atoms in the ground state and the excited state respectively, A and B are the Einstein A and B coefficients, $\rho(\omega)$ is the angular frequency dependent energy density of the incoming laser pulse in the interval ω to ω+dω and $s(\omega)$ is the angular frequency dependent probability density of a transition in the interval ω to ω+dω.

First, a suitable estimate for these variables must be found before the coupled differential equations can be solved. The values for the Einstein A and B coefficients can be found first. A_{21} is the Einstein A coefficient for the spontaneous emission from the excited state to the ground state. B_{21} is the Einstein B coefficient for the stimulated emission from the excited state to the ground state. B_{12} is the Einstein B coefficient for absorption of photons causing atoms to excite from the ground state to the excited state. These values are related by the formulae in Equation 2.22 [22].

For the transition $4s^2\ {}^1S_0 \rightarrow 4s4p\ {}^1P_1{}^o$, $A_{21} = 7.14 \times 10^8\ s^{-1}$ [16]. Using Equations 2.22, $B_{21} = 2.6 \times 10^{21}\ m{\cdot}kg^{-1}$ and $B_{12} = 3 \times B_{21} = 7.9 \times 10^{21}\ m{\cdot}kg^{-1}$ for $\lambda = 213.857351$ nm.

The other variables, the density of the Zn, the transition profile and the beam profile, will be calculated in the next three subsections.

4.3.1 Density

To set up the rate equations, the density of the Zn atoms in the sample, before the laser beam is applied, needs to be calculated. All the atoms are assumed to be in the ground state initially. Before working out the density of the Zn atoms, the temperature of the atoms needs to be found. Finding the temperature of the atoms serves two purposes: it is used to find the density of the atoms as well as the Doppler broadened transition probability distribution.

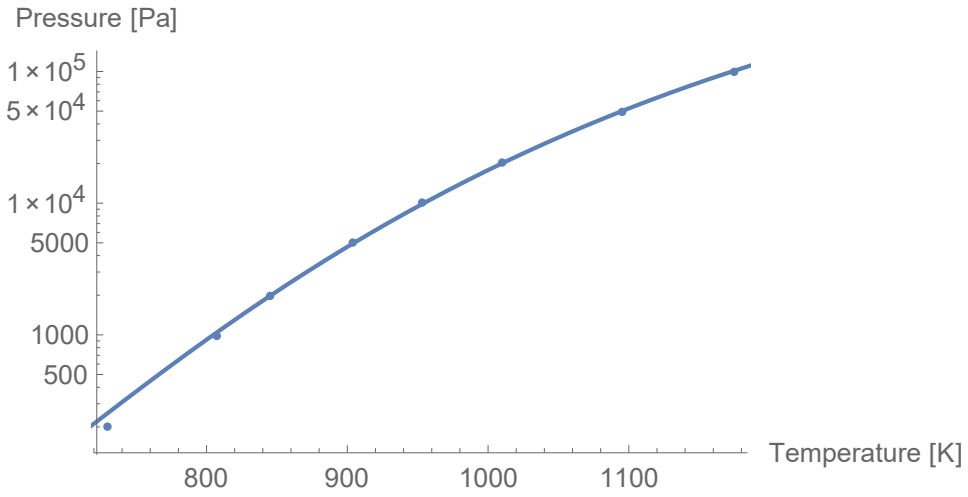

Figure 4.5: Data from Kaye and Laby Tables of Physical and Chemical Constants [4] for Na vapour pressures at different temperatures and fit of data using modified Antoine Equation, Equation 2.1.

The Zn pressure is measured indirectly using the following method: First, the pressure of the Ar that is in contact with the Na vapour in the vertical part of the heat pipe is measured. When phase equilibrium has been reached between the liquid and vapour of Na in the vertical heat pipe, it means that the vapour pressure of the Na is equal to the pressure of the Ar (property of boiling). Then, using the pressure-temperature curve for Na, the temperature of the Na in the vertical pipe can be determined. Because the Na in the vertical pipe envelopes the horizontal pipe, the Zn in the horizontal heat pipe is assumed to have the same temperature as the Na. Then, using the temperature-pressure curve for Zn, the pressure of the Zn vapour can be determined. The method for finding the pressure of the Zn vapour in the horizontal pipe via the pressure of the Ar in the vertical pipe is illustrated in Figure 2.3.

For the most prominent experiment, the Ar buffer gas in the vertical pipe was measured to be 260 Torr, which is equivalent to 35 kPa. This is the same as the pressure of the Na vapour. Then, to construct a temperature vs pressure curve for Na, data from Kaye and Laby Tables of Physical and Chemical Constants [4] was used. This data is then fitted using the imperial modified Antione Equation, Equation 2.1. The data and fit are shown in Figure 4.5 and the resulting values for the Antoine coefficients, a, b, c and d are given in Table 4.2.

	Estimate	**Standard Error**
a	73.8982	12.7071
b	-16 510.6	2 410.24
c	-18.0921	3.52928
d	1.13986×10^9	2.90604×10^8

Table 4.2: Fitted values for the Antoine coefficients for the Na temperature vs pressure curve.

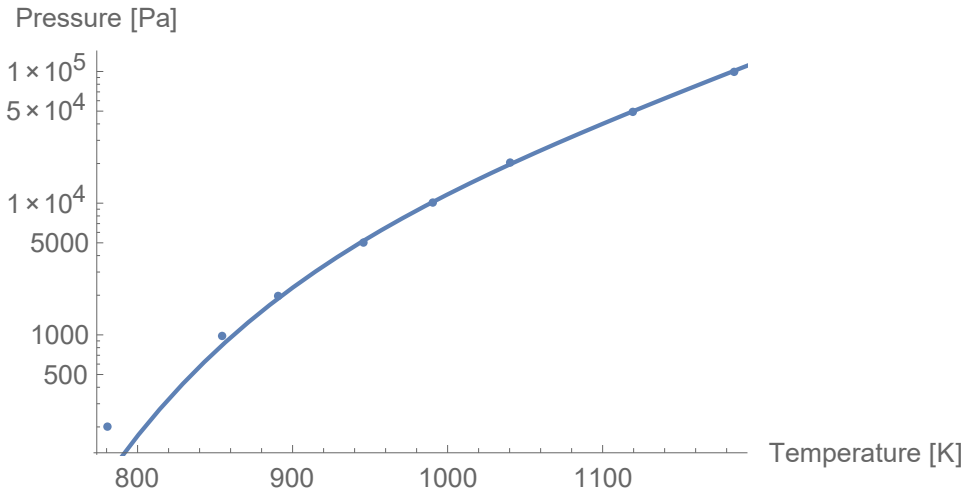

Figure 4.6: Data from Kaye and Laby Tables of Physical and Chemical Constants [4] for Zn vapour pressures at different temperatures and fit of data using modified Antoine Equation, Equation 2.1.

Using the fit, it is found that the temperature of Na corresponding to 35 kPa is 1060 K. Since the Na and the Zn are at the same temperature, the temperature of the Zn is also 1060 K. Now the corresponding pressure of Zn can be determined. The same method as in the case of Na is used. The pressure-temperature curve is found by fitting the modified Antione Equation to data from Kaye and Laby Tables of Physical and Chemical Constants [4]. The data and fit are displayed in Figure 4.6 and the Antoine coefficients, a, b, c and d are presented in Table 4.3.

	Estimate	**Standard Error**
a	-222.667	87.9787
b	38 295.8	17 111.3
c	64.6125	24.3537
d	-5.39902×10^9	2.1923×10^9

Table 4.3: Fitted values for the Antoine coefficients for the Zn temperature vs pressure curve.

From the pressure-temperature curve in Figure 4.6 it is found that the corresponding pressure for Zn at 1060 K is 25 kPa.

Now that the pressure as well as the temperature of the Zn in the horizontal section of the heat pipe is known, an estimate for the number density of the Zn atoms can be made. To do this, the ideal gas law is used as seen in Section 2.4.2. Using the values calculated for the temperature and the pressure of the Zn atoms, the number density of the atoms is calculated to be 1.7×10^{24} atoms per m^3.

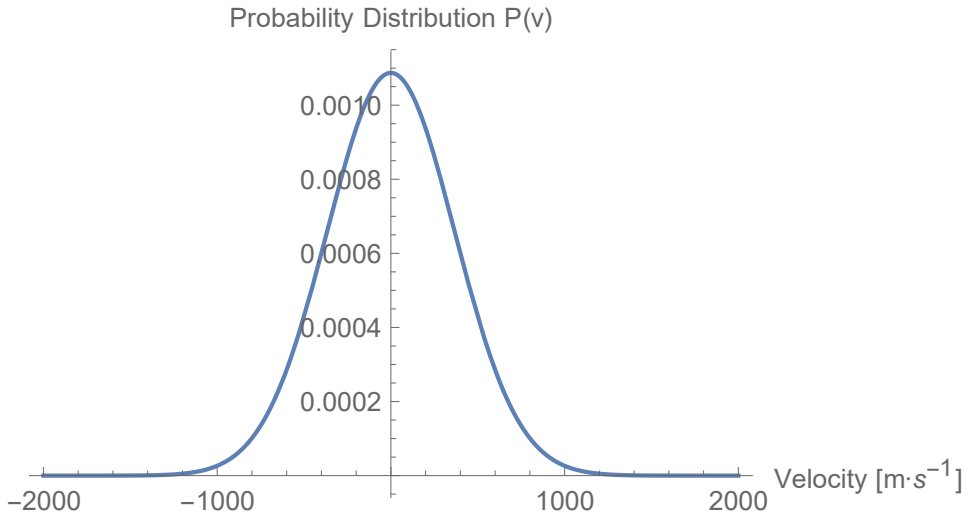

Figure 4.7: One dimensional velocity dependent Maxwell-Boltzmann probability distribution.

4.3.2 Transition Profile

The next variable that needs to calculated is the transition profile of the transition from the ground state $4s^2\ {}^1S_0$ to the excited state $4s4p\ {}^1P_1{}^o$. There are a few factors that contribute to the width of the transition line. The first is the natural line width which cannot be decreased by lowering the temperature, pressure or ambient electromagnetic interference. The natural line profile is estimated to be Lorentzian. This contribution to the line width is insignificant when compared to the contribution due to Doppler broadening and collisions. Calculating the effect of collisions on the line shape is out of the scope of this project. Nevertheless, the effect of Doppler broadening on the line profile can be calculated.

Doppler broadening is very significant and occurs because the sample inside a heat pipe has a very high temperature. Doppler broadening is dependent on the velocities of the atoms inside the heat pipe, but it only depends on velocities in the direction of the laser beam. Therefore, to model the velocities of the atoms in the heat pipe, the Maxwell-Boltzmann Distribution in one dimension, Equation 2.10, will be used.

Using the natural mass of Zn as $1.0856603 \times 10^{-25}$ kg and the calculated temperature of 1060 K, the Maxwell-Boltzmann distribution shown in Figure 4.7 is calculated. From Figure 4.7 it is clear that the mean velocity is zero, as expected.

Using the Maxwell-Boltzmann distribution as well as the Doppler theory the Doppler broadened angular frequency dependent line shape, $s(\omega)$ (Equation 2.13), is found, as plotted in Figure 4.8. The FWHM in angular frequency of $s(\omega)$ is $\text{FWHM}_s = 2.5 \times 10^{10}$ rad/s.

The Doppler broadened angular frequency dependent line shape, $s(\omega)$, plotted in Figure 4.8, is plotted using the natural mass of Zn as $1.0856603 \times 10^{-25}$ kg and calculated temperature of 1060 K. The central angular frequency is 8.8×10^{15} rad/s. This comes from the central wavelength of the $4s^2\ {}^1S_0 \rightarrow 4s4p\ {}^1P_1{}^o$ given as 213.857351 nm [16].

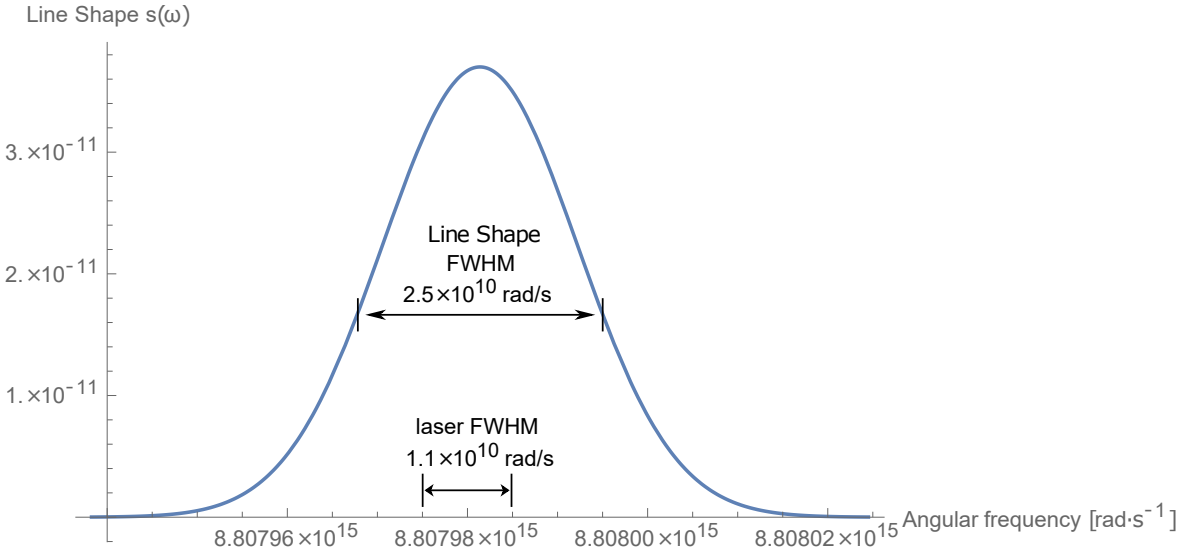

Figure 4.8: Doppler broadened line shape, $s(\omega)$.

4.3.3 Laser Pulse Profile

In order to calculate the rate equations, the energy density distribution, $\rho(\omega)$, of the laser pulse incident on our sample needs to be found first. To find $\rho(\omega)$, the laser bandwidth, that is specified in the laser manual as the Full Width at Half of the Maximum (FWHM) of the laser's emitted spectrum is used. A Lambda Physik dye laser is used. It is specified to have a FWHM of 0.04 cm^{-1} for the wavelength region around 428 nm. A FWHM of 0.04 cm^{-1} translates to a FWHM of 1.2×10^9 Hz in frequency or 7.5×10^9 rad·s^{-1} in angular frequency.

Directly after the laser beam exits the Lambda Physik dye laser, the beam undergoes Second Harmonic Generation (SHG) in order to generate the needed 8.8×10^{15} rad·s^{-1} (213.9 nm) beam. In Section 2.6 it is shown that the FHWM of the beam decreases by a factor $\sqrt{2}$ during SHG due to the intensity being squared during SHG. The FWHM also increases by a factor of 2 because the frequency doubles. Therefore, SHG effectively increases the FWHM by $\sqrt{2}$, resulting in a FWHM $= 1.1 \times 10^{10}$ rad·s^{-1} after SHG.

The intensity of the laser beam also needs to be found. The detector can measure the pulse energy of the beam before the SHG, but not after. Before SHG the laser beam has a per pulse energy (E_L) of 0.3 mJ. For SHG a β-Barium Borate (BBO) crystal with Type 1 phase matching is used. Rahman, A. et al. calculated the theoretical efficiency of BBO crystals in a 2018 paper [21]. Using their results, the conservative figure of 10% efficiency (η_SHG) is used. The amount of transmission for each optic in the experimental setup (Figure 3.3) for 213.9 nm is calculated using Fresnel equations and data from Thorlabs, resulting in an effective net transmission of all optics in the path (T_net) of 6%. To find the intensity, in W/m^2, the per pulse energy needs to be divided by the pulse duration (τ_L) and spacial beam area (A_L). The laser beam has a

pulse duration of 8 ns and the beam has a radius of 1 mm. After the beam has passed through the various optics, the laser beam incident on our sample has an estimated intensity of 7.5×10^8 W/m^2 as calculated in Equation 4.1.

$$\begin{aligned} I &= \frac{\mathrm{E_L}\eta_{\mathrm{SHG}}\mathrm{T_{net}}}{\tau_{\mathrm{L}}\mathrm{A_L}} \\ I &= (0.003 \times 0.1 \times 0.06)/(8 \times 10^{-9} \times \pi \times 0.001^2) \\ I &= 7.5 \times 10^8\ \mathrm{W/m^2} \end{aligned} \tag{4.1}$$

There are two intensities that are important when calculating $\rho(\omega)$. The first is the intensity of the central wavelength and the second is the integrated intensity over all wavelengths. The detector being used, a Coherent laser energy meter, is not wavelength selective. It measures the pulse energy integrated over a large wavelength range. Therefore, the intensity calculated in Equation 4.1 is considered to be the total intensity integrated over all wavelengths. The relation between the total intensity, I, and the total energy density, ρ, is shown in Equation 4.2.

$$\rho = \int_{-\infty}^{\infty} \rho(\omega)\mathrm{d}\omega = \int_{-\infty}^{\infty} \frac{I(\omega)}{c}\mathrm{d}\omega = \frac{I}{c} \tag{4.2}$$

In Equation 4.2, $\rho(\omega)$ is the energy density for the angular frequency interval ω to ω+dω measured in J·s·m^{-3}·rad^{-1}, $I(\omega)$ is the intensity for the angular frequency interval ω to ω+dω measured in W·s·m^{-2}·rad^{-1} and c is the speed of light in m·s^{-1}. The integrals were evaluated as the total energy density in J·m^{-3}, $\rho = \int_{-\infty}^{\infty} \rho(\omega)\mathrm{d}\omega$, and the total intensity in W·m^{-2}, $I = \int_{-\infty}^{\infty} \frac{I(\omega)}{c}\mathrm{d}\omega$.

The goal is to find $\rho(\omega)$. It is approximated as a Gaussian, $\rho(\omega) = ae^{\frac{-(\omega-\omega_0)^2}{2\sigma^2}}$, where σ is the standard deviation, ω_0 is the central frequency and a is the peak energy density, $a = \rho(\omega_0)$. The total energy density is given by the integral,

$$\rho = \int_{-\infty}^{\infty} \rho(\omega)\mathrm{d}\omega = \sqrt{2\pi}a|\sigma| = \frac{I}{c}. \tag{4.3}$$

Here, σ is the standard deviation of the Gaussian. σ and FWHM are related by $\sigma = \mathrm{FWHM}/\sqrt{8\ln 2}$. The FWHM is calculated to be 1.1×10^{10} rad·s^{-1}. Now, a can be solved. This is shown in Equation 4.4.

$$\begin{aligned} a &= \frac{I/c}{\sqrt{2\pi}\sigma} \\ &= \frac{(I/c)\sqrt{8\ln 2}}{\sqrt{2\pi}FWHM} \\ &= 2.2 \times 10^{-10}\ \mathrm{J \cdot s \cdot m^{-3} \cdot rad^{-1}} \end{aligned} \tag{4.4}$$

$\rho(\omega)$ can now be plotted, as shown in Figure 4.9.

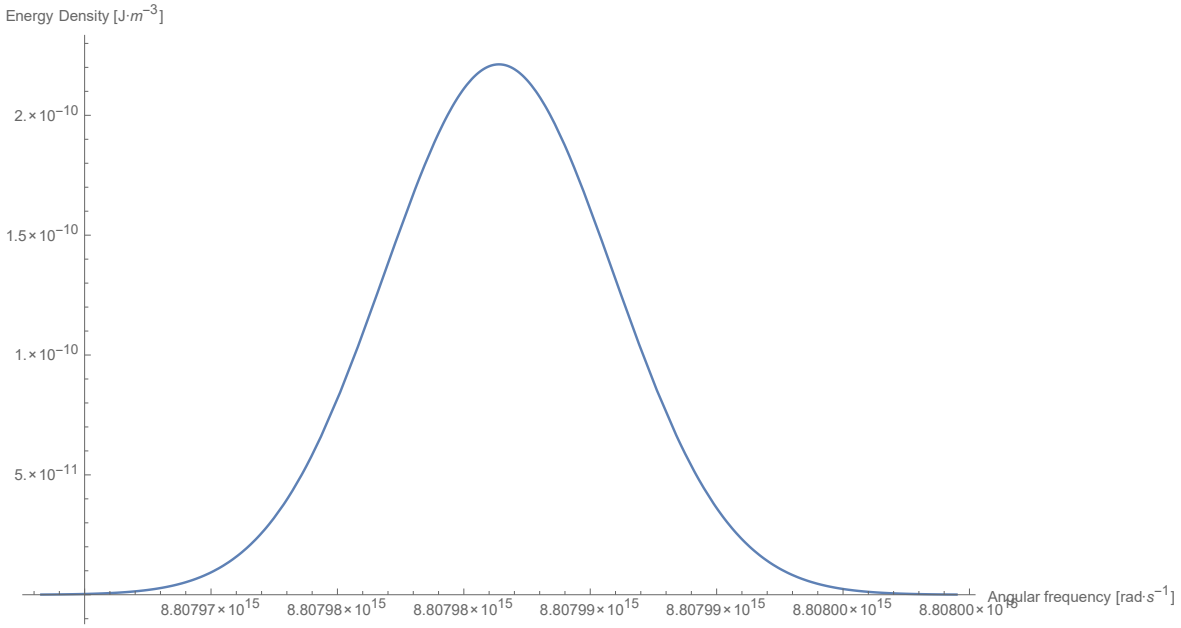

Figure 4.9: Angular frequency dependant energy density, $\rho(\omega)$, of the dye laser beam at the position of the sample.

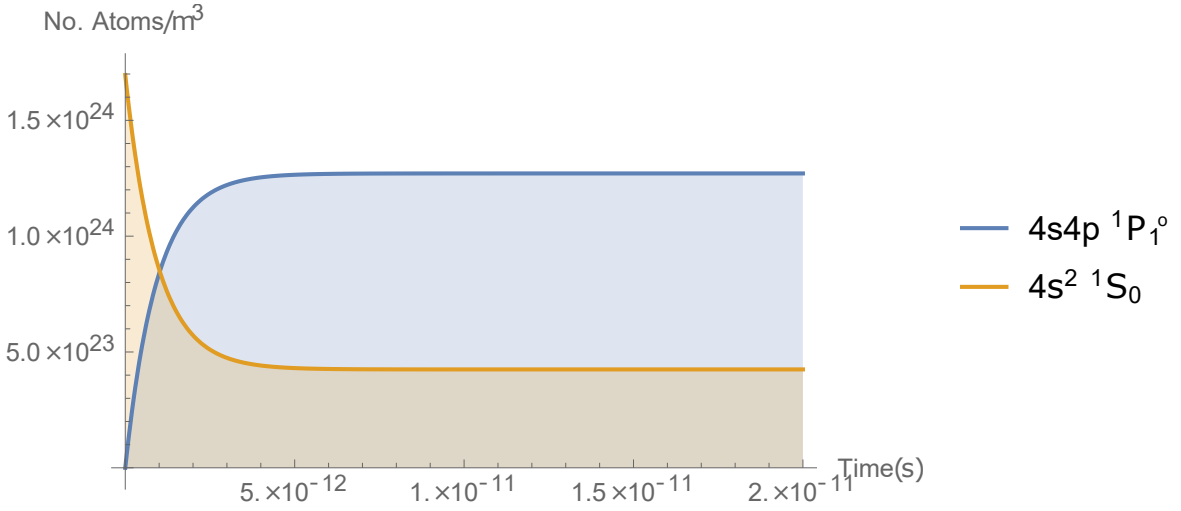

Figure 4.10: Einstein rate equation, modelling the population in the ground state $4s^2\ {}^1S_0$ and the excited state $4s4p\ {}^1P_1{}^o$ over time, using a time independent $\rho(\omega)$.

4.4 Rate Equations

The Einstein A and B coefficients, density of Zn atoms, transition profile, $s(\omega)$ and the beam profile, $\rho(\omega)$ have all been determined. Now, the rate equations from Equation 2.20 can be evaluated. Substituting these functions and values, the dynamics of the population on the ground state $4s^2\ {}^1S_0$ and the excited state $4s4p\ {}^1P_1{}^o$ are found and are plotted in Figure 4.10.

As seen in Figure 4.10, the population comes to a steady state after a time of about 5 ps. Here, a constant laser energy density $\rho(\omega)$ that does not change over time, is

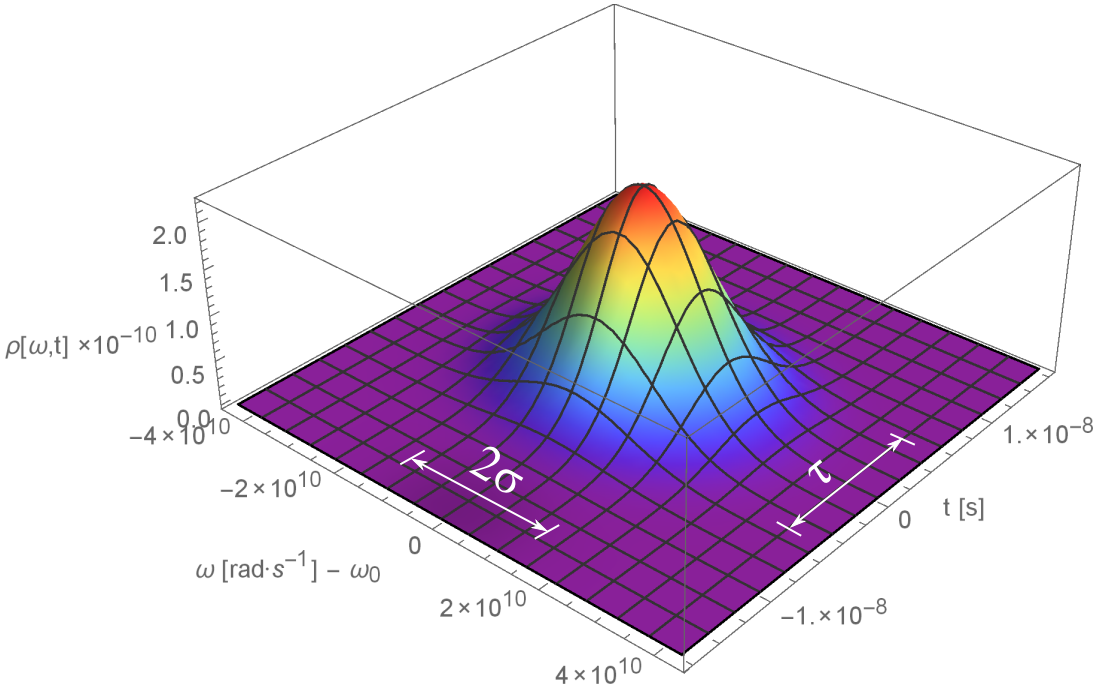

Figure 4.11: Theoretical angular frequency and time dependent energy density $\rho(\omega, t)$ of the laser pulses that reach the sample, with the FWHM pulse duration, τ, and the standard deviation of the frequency profile, σ, indicated.

assumed. The upper state, N_2, reaches a population density of $N_2 \approx 1.27 \times 10^{24}$ atoms per m^3 in the steady state. The ratio of the upper state to the total population density is $N_2 \approx \frac{1.27\times10^{24}}{1.7\times10^{24}} N = 0.747N$ which is close to the saturation limit of $N_2 = \frac{3}{4}N$, as discussed in Section 2.10. This means that the transition is saturated, using an intensity of 7.5×10^8 W/m^2.

The laser pulse for this experiment has a temporal width of only 8 ns. A more accurate depiction of the population dynamics can be modelled by taking this into account. The angular frequency and time dependent energy density $\rho(\omega, t)$ is plotted in Figure 4.11 where the pulse duration at the central frequency is assumed to be a Gaussian with a FWHM of 8 ns.

Using a time dependent $\rho(\omega, t)$ instead of the time independent $\rho(\omega)$ the rate equations provide the population dynamics shown in Figure 4.12. The populations do not remain in the steady state for long after the pulse, due the lifetime of the excited state being only 1.4 ns. Also seen in Figure 4.12, for intensity, I, the atoms seem to be excited before significant laser pulse intensity is present. The reason for this is that the laser pulse is much more intense than is needed for saturation and the Gaussian function never reaches zero. The actual laser pulse energy starts from zero and goes back to zero. In the future one may use a different function to model the laser pulse.

Also seen in Figure 4.12 is the population dynamics for saturation intensity, $\mathrm{I}_{sat} = 5.0 \times 10^5$ W/m^2 $= 0.0008\, I$, given by Equation 2.26. This is less than the actual intensity, I, that the laser beam has. The population dynamics for $35 \times I_{sat} = 0.03I =$

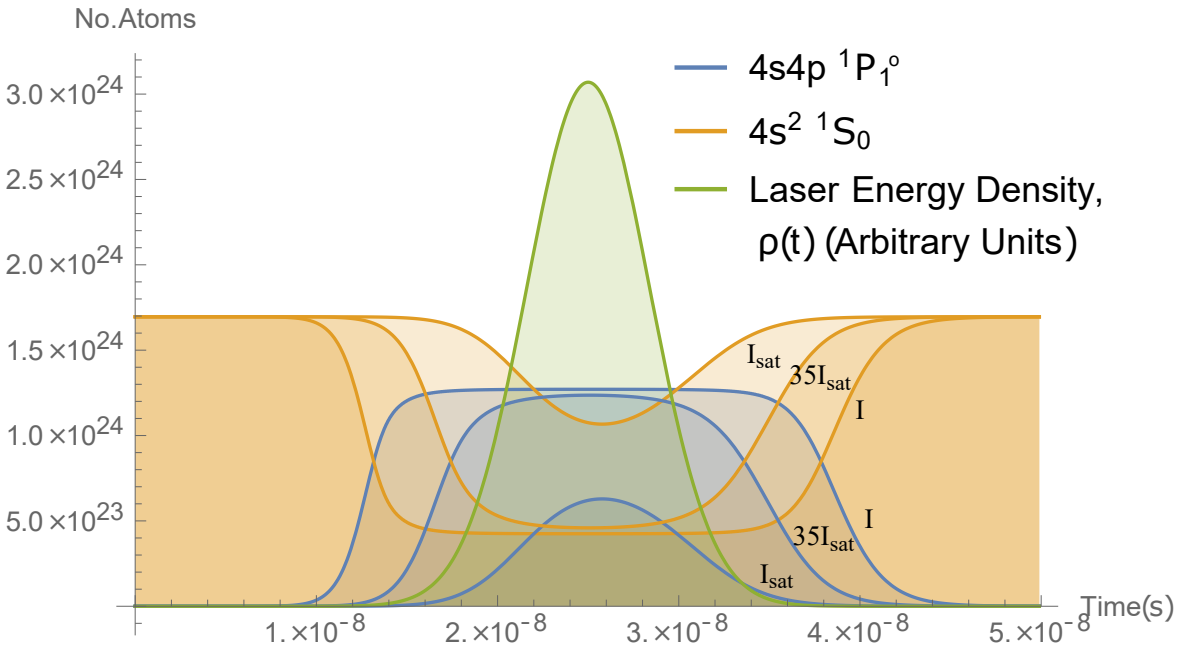

Figure 4.12: Einstein rate equation, modelling the population in the ground state $4s^2$ $^1S_0$ and the excited state 4s4p $^1P_1{}^o$ over time, using a time dependent $\rho(\omega, t)$. The upper and lower state populations are shown for the experimental laser intensity, I, the saturation intensity, I_{sat}, and for $35I_{sat}$.

2×10^7 W/m^2 is also shown in Figure 4.12. The Equivalent energy densities for these intensities are shown in Equations 4.5 - 4.7. At the actual intensity, I, the peak value of N_2 is $N_2 = 0.747N$. This is close to the limit value, meaning that saturation of the transition is achieved. An upper state population of $N_2 \approx 0.74N$ is maintained for approximately 16 ns. At an intensity of $35I_{sat} = 0.03I$, the maximum value is $N_2 = 0.73N$. The transition is not completely saturated and a high N_2 population is only maintained for about 8 ns. At intensity, I_{sat}, the maximum N_2 population is only about half of the limit value.

$$I_{sat} = 5.0 \times 10^5 \text{ W/m}^2 \implies \rho_{sat} = \frac{I_{sat}}{c} = 0.002 \text{ J/m}^3 \quad (4.5)$$

$$35I_{sat} = 2 \times 10^7 \text{ W/m}^2 \implies 35\rho_{sat} = 35\frac{I_{sat}}{c} = 0.06 \text{ J/m}^3 \quad (4.6)$$

$$I = 7.5 \times 10^8 \text{ W/m}^2 \implies \rho = \frac{I}{c} = 2.5 \text{ J/m}^3 \quad (4.7)$$

The dynamics are different for a transition from the ground state to a longer lived state like the forbidden triplet state 4s4p $^3P_1{}^o$. This transition has an Einstein A coefficient of $A_{21} = 3.8 \times 10^4$ s^{-1} [16], which results in a lifetime of 2.6×10^{-5} s. To excite this transition the dye laser would need to output 615 nm. Rhodamine B would be a good choice of dye for this wavelength, becuase the peak intensity of the dye is close to this wavelength. In addition, it is a very durable dye and does not need to be replaced as often as Stilbene 3. The laser has a reported bandwidth of 0.03 nm for this wavelength. The decays from 4s4p $^3P_1{}^o$ to 4s4p $^1P_1{}^o$ are being ignored, because this is a forbidden

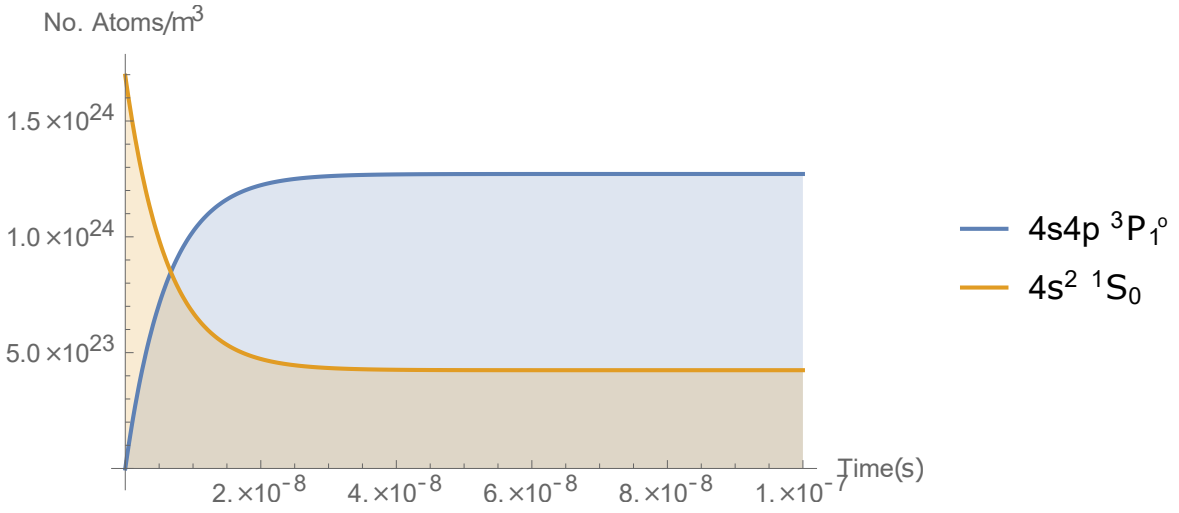

Figure 4.13: Einstein rate equation, modelling the population in the ground state $4s^2\ {}^1S_0$ and the excited state $4s4p\ {}^3P_1{}^o$ over time using a time independent $\rho(\omega)$.

transition. Other than this, the only decay available is to the ground state. Therefore, a two state system is once again assumed.

The population dynamics of the ground state and excited state in the case of excitation to triplet $4s4p\ {}^3P_1{}^o$ state, by continuous radiation $\rho(\omega)$, are shown in Figure 4.13. The excited state takes much longer to reach equilibrium here, due to the fact that the state is forbidden. It takes about 30 ns to reach equilibrium with a constant energy density. At equilibrium, $N_2 \approx 0.75N$, meaning saturation of the transition has been reached.

The dynamics with a time dependent energy density are shown in Figure 4.14. The dynamics are shown for the estimated energy density, ρ, that reaches the sample, 20% of the estimated energy density, 0.2ρ, and 10% of the estimated energy density, 0.1ρ. Unlike the singlet-singlet transition, the estimated energy density, ρ, is close to saturating the singlet-triplet transition, but is not great enough to saturate the transition. After the pulse the excited state has two thirds as much population as the total population ($N_2 \approx 0.66N$), but if the transition was saturated the excited state would have three quarters as much population as the total population after the pulse ($N_2 \approx 0.75N$). As for 0.1ρ, 0.2ρ, they do not come close to saturation.

However, for all energy density values, populations remain in the steady state for much longer, allowing time for a second or third pulse to excite other transitions or ionise, using the population in the $4s4p\ {}^3P_1{}^o$ state.

4.5 Absorption

The aim is to measure the amount of absorption in the heat pipe experimentally, using Atomic Absorption Spectroscopy (AAS). This method makes a measurement of the intensity of the beam before and after the sample (Zn inside the heat pipe). The de-

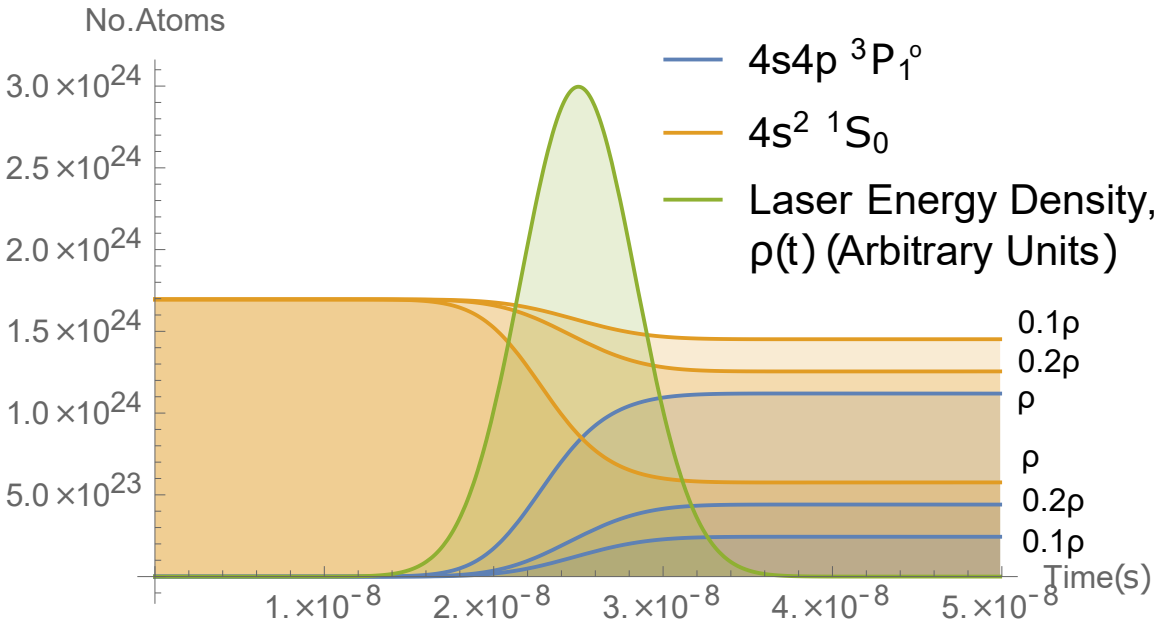

Figure 4.14: Einstein rate equation, modelling the population in the ground state $4s^2\ {}^1S_0$ and the excited state $4s4p\ {}^3P_1{}^o$ over time using a time dependent $\rho(\omega, t)$.

crease in intensity is due to absorption.

Before the experiment, the amount of absorption can be calculated. However, before the absorption can be calculated, the absorption cross-section needs to be calculated. This can be calculated using one of three assumptions. A narrowband approximation can be made, which is applicable when the laser frequency bandwidth (FWHM_ρ) is much narrower than the frequency bandwidth of the transition (FWHM_s). This becomes useful when the laser profile is narrow, but unknown, as the absorption under the narrowband approximation does not depend on the laser pulse (as derived in Equation 2.28).

The other approximation is the broadband approximation, which is applicable when the laser frequency bandwidth is much broader than the frequency bandwidth of the transition. This becomes useful when the transition profile is narrow, but unknown, as the absorption under the broadband approximation does not depend on the transition profile (as derived in Equation 2.30).

Finally, the rate equations can be used with no approximations. This is useful when the laser bandwidth and the transition bandwidth are of the same order. Regardless of the transition profile and the laser bandwidth profile, this method should give the best results at the cost of knowing both the laser pulse profile as well as the transition profile.

For the simulation of the $4s^2\ {}^1S_0 \rightarrow 4s4p\ {}^1P_1{}^o$ transition, $\text{FWHM}_\rho = 1.1 \times 10^{10}$ rad·s^{-1} and $\text{FWHM}_s = 2.5 \times 10^{10}$ rad·s^{-1}. Which means, $\text{FWHM}_\rho < \text{FWHM}_s$. Therefore, either the narrowband or general relation could be valid. The broadband approximation is not valid. Table 4.4 shows results for the narrowband approximation and the general relation.

Approximation	Equation	Result
Narrowband Approximation [22]	$\sigma = A_{21}\frac{\lambda^2}{4}s(\omega_0)$	$\sigma = 3.0 \times 10^{-16}\ \mathrm{m}^2$
General Relation (derived in Section 2.26)	$\sigma(\omega) = A_{21}\frac{c\lambda^2}{4I}\int_{-\infty}^{\infty}\rho(\omega)s(\omega)\mathrm{d}\omega$	$\sigma = 3.3 \times 10^{-16}\ \mathrm{m}^2$

Table 4.4: Calculated absorption cross-sections for the narrowband approximation and general relation.

From the results it is evident that the narrowband approximation provides the lower limit, as expected, and using the general relation produces a more accurate estimate for the absorption cross-section.

Using the calculated cross-section value, the amount of absorption expected in the sample can be calculated using the Beer Lambert law or via rate equations. The Beer Lambert law assumes an intensity much lower than the saturation intensity, see Section 2.8, i.e. $I << I_{sat}$. The rate equations do not make such assumptions. Therefore, the intensity that is being used needs to be compared to the saturation intensity to determine if the Beer Lambert law will be useful for this simulation.

Using the formula for the saturation intensity, Equation 2.26, the saturation intensity is calculated to be $I_{sat} = 5.0 \times 10^5\ \mathrm{W/m^2}$. Note that Equation 2.26 has been derived for narrowband light tuned onto resonance. Therefore, the actual saturation intensity will be larger than the calculated value as not all of the laser bandwidth is exactly on resonance. The intensity from the simulation is $I = 7.5 \times 10^8\ \mathrm{W/m^2}$. This does not fulfil the requirement of $I << I_{sat}$. Therefore, the Beer Lambert law is expected to give a lower limit for the absorption and the absorption calculated using the rate equations to give a higher and more accurate estimate. The rate equation model for quantifying absorption is discussed in Section 2.9.

The fraction of absorption is defined in Equation 4.8. If the intensity, $I(L)$, after the sample ($L = 6$ cm) is half that of the intensity, $I(0)$, before the sample, there is 50% absorption or $f_{abs} = 0.5$. The results for both assumptions (Beer Lambert Law and Rate Equation Model) are shown in Table 4.5 with equations from Section 2.26.

$$f_{abs} = \frac{I(0) - I(L)}{I(0)} \tag{4.8}$$

As expected, using the Beer Lambert Law showed more absorption than using the rate equations. However, in both calculations the absorption is approximately 1, meaning that the light is on resonance and it will be absorbed completely.

It will be of useful for future experiments to find the temperature and intensity needed for 50% absorption ($f_{abs} = 0.5$). For this reason, Figure 4.15 plots the absorbed fraction

Model	Equation	Result
Beer Lambert Law (Assumes $I << I_{sat}$)	$f_{abs} = 1 - e^{-\sigma N z}$	$f_{abs} = 1 - 5.2 \times 10^{-14703886}$
Rate Equation Model	$f_{abs} = 1 - \frac{I(L)}{I(0)}$	$f_{abs} = 1 - 3.0 \times 10^{-98}$

Table 4.5: Calculated absorption using Beers Law and rate equations, where $I(L)$ is found by solving Equation 2.31 numerically using Mathematica.

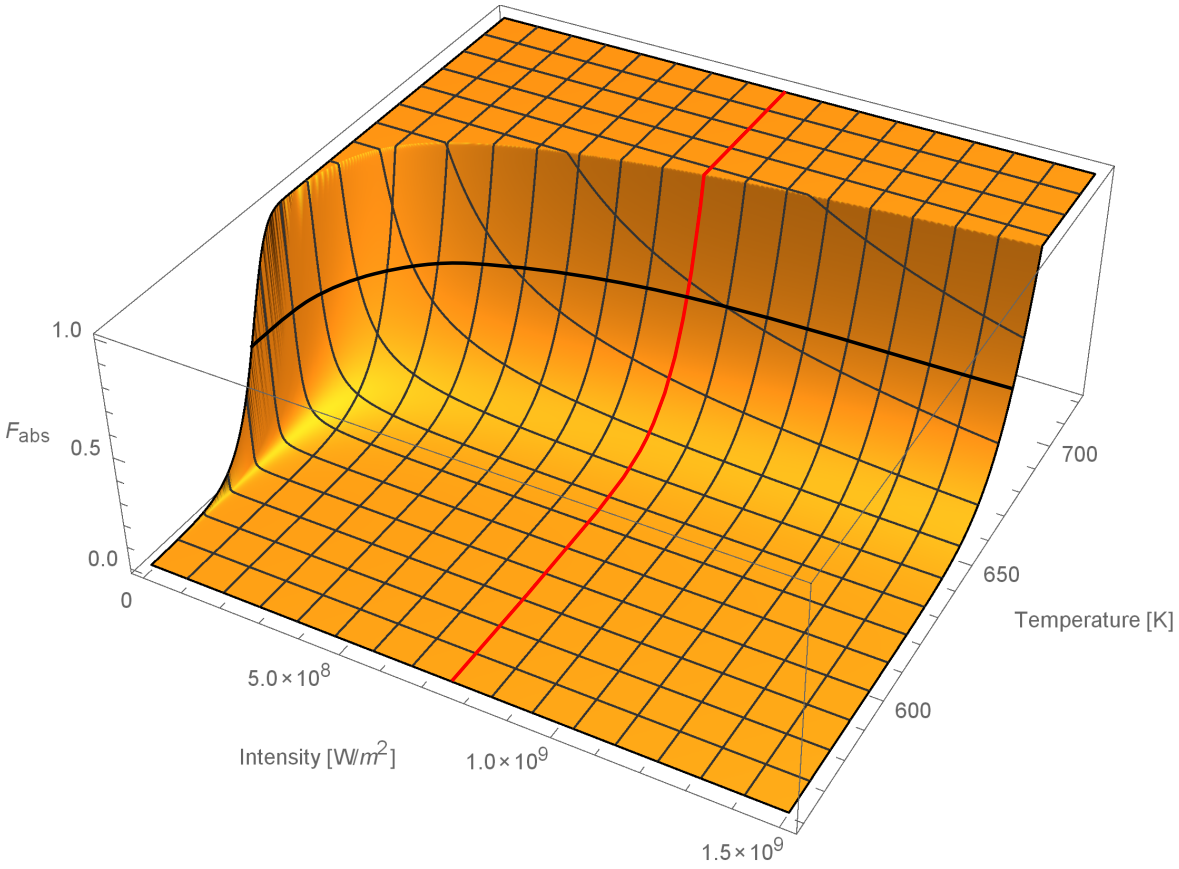

Figure 4.15: Fraction of absorption (f_{abs}) vs Intensity and Temperature, where, $f_{abs} = \frac{I(0)-I(L)}{I(0)}$. $I(0)$ is the intensity on the x-axis and $I(L)$ is found by solving Equation 2.37 numerically using Mathematica.

for intensities from 1 to 2*I and for temperatures between 560 K and 720 K.

The black line in Figure 4.15 indicates the contour on which the absorption is 50%. The red line shows where the intensity is I = 7.5 × 10^8 W/m^2. The intersection of these lines would be the ideal experimental setup, because neither I(0) nor I(L) is small, there is a significant difference between I(L) and I(0) and complete absorption of all

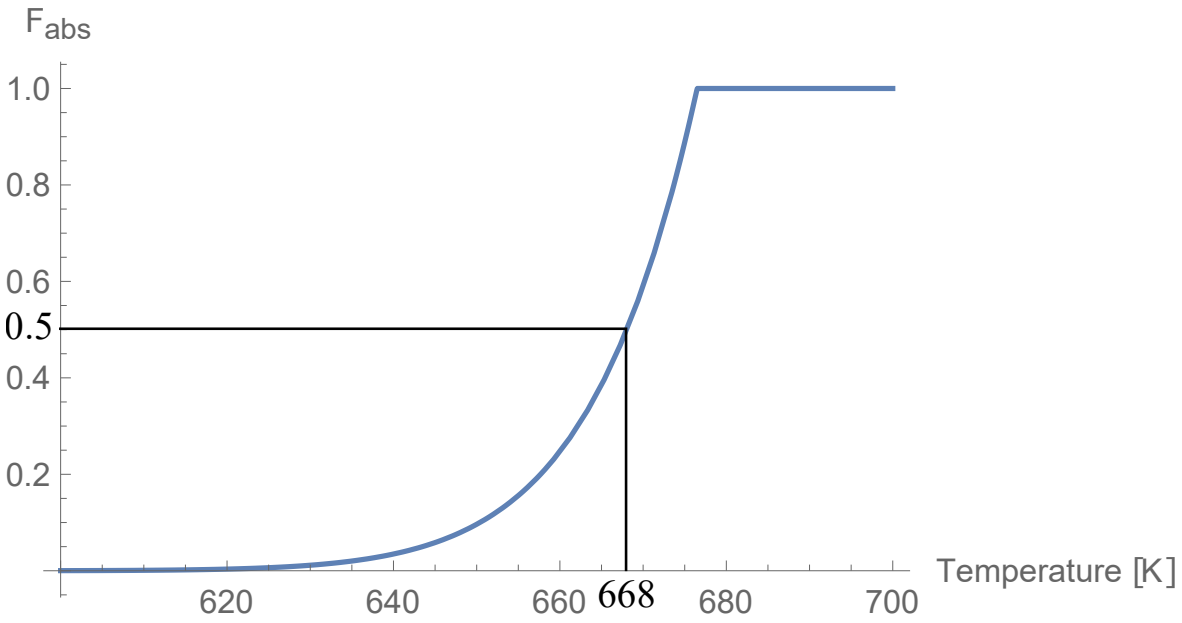

Figure 4.16: Fraction of absorption vs Temperature for I = 7.5 × 10^8 W/m^2.

light is avoided. The lineout of the red line is shown in Figure 4.16.

The temperature of 668 K for the Zn would produce 50% absorption, using an intensity of I = 7.5 × 10^8 W/m^2. From here, the pressure needed in the vertical pipe for 50% absorption can be found. The Zn and the Na are at the same temperature. Using the Na pressure vs temperature curve a pressure of 79 Pa = 7.8 ×10^{-4} bar is found. This pressure is very low and it still has to be determined whether the heat pipe can function at such low pressure.

4.6 Experimental Results

This is a proof of principle experiment to determine the feasibility of doing absorption spectroscopy with a time delayed reference laser pulse and the signal pulse and reference pulse measured by the same detector. Therefore, maximal absorption in the heat pipe is sought. This is achieved by increasing the pressure in the heat pipe to 560 Torr = 7.4 ×10^4 Pa = 0.74 bar. A pressure above 1 bar was avoided due to the chamber being only tested under low pressure conditions.

Using the experimental setup in Figure 3.3, absorption of the 213.9 nm line of Zn in the heat pipe was found. Oscilloscope traces are recorded for a scan from 212.4 nm to 215.5 nm using a step-size of 0.03 nm and an average of 64 pulses per measurement. A custom program in Python was written by the author to analyse the recorded traces (See Appendix for code). In Figure 4.17, two selected traces are shown, one off resonance (blue) and one on resonance (orange). The first peak in the blue section is the pulse that propagated through the sample, whereas the second peak, in the orange section, is the delayed reference pulse. In the on resonance curve the sample pulse decreased

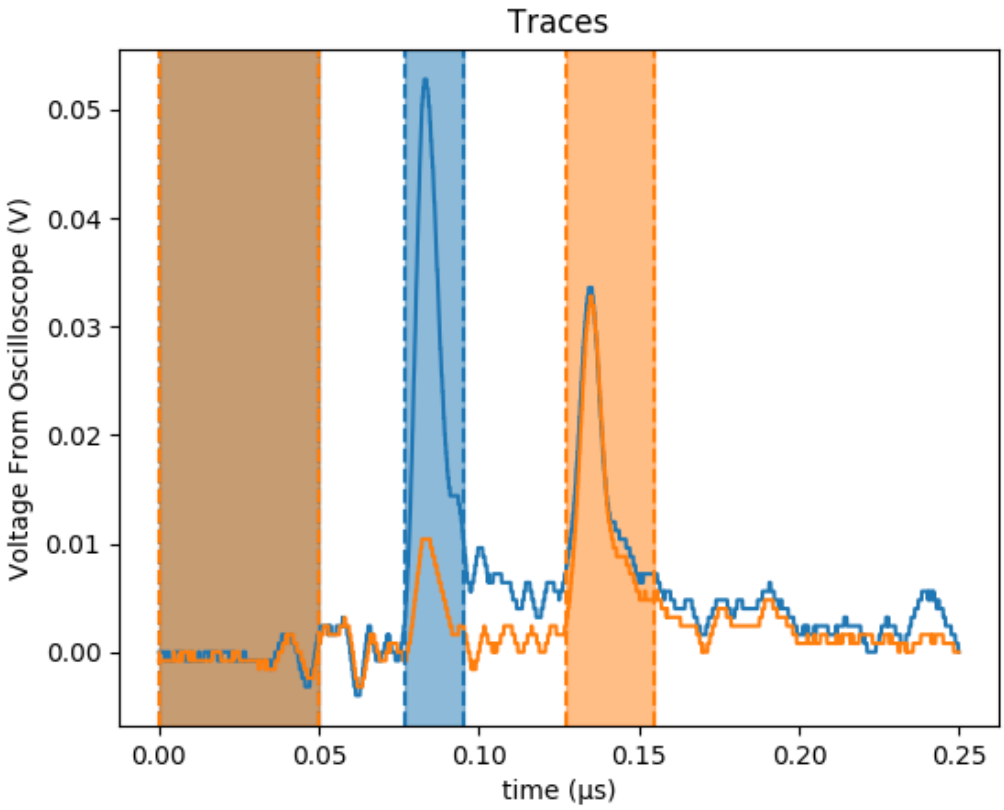

Figure 4.17: Oscilloscope traces of the beam going through the heat pipe (left) and the beam that is being delayed and does not go through the heat pipe (right) for selected second harmonic wavelengths 213.76 nm (orange curve) and 214.39 nm (blue curve).

compared to the off resonance curve, while the reference pulse remained constant. The decrease in the sample beam is due to absorption.

There are three sections highlighted in Figure 4.17. The first section, from the left, is what is used to determine the background. The background changes slightly after each scan, so for each scan the average of this section is found and subtracted from the whole trace in order to calculate the peak areas. The next two sections, the blue and orange sections, were integrated using the Simpsons method to determine the area under the two peaks respectively. The output of the program is the areas of the two peaks as a function of incident laser wavelength, as depicted in Figures 4.18 and 4.19

As seen in Figure 4.17, the sample and reference peaks have overlapping features. This is far from ideal. The first peak is the one that goes through the heat pipe and decreases due to absorption. Since the peaks overlap, the second peak will also decrease slightly when there is absorption. This negative effect can be eliminated in future experiments by having the delayed pulse go through the heat pipe and the other pulse not. Therefore the second peak will decrease due to absorption and will not affect the first peak.

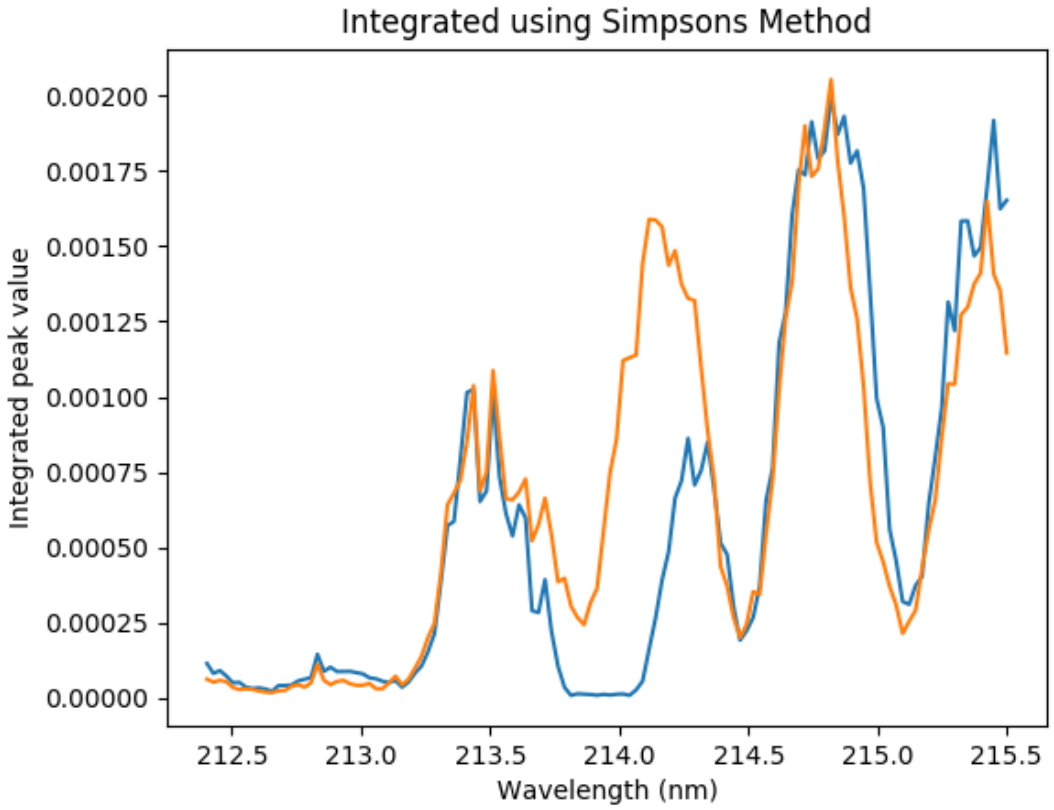

Figure 4.18: Integration over both peaks. The integrated peak areas of the sample beam passing through the heat pipe (blue) and the delayed reference beam (orange) as a function of laser wavelength.

The first peak will still affect the second peak though, due to the overlap. However, the amount of overlap can by decreased by decreasing the intensity of the beam. But in doing this, the signal-to-noise ratio will decrease. This is not ideal, since the noise is large compared to our signal as seen in Figure 4.19.

Figure 4.18 shows the peak areas versus incident wavelength. In the centre of the scan at 213.9 nm the blue graph (the peak area of the sample beam that goes through the heat pipe) decreases significantly compared to the orange graph (the peak area of the reference beam). This is due to absorption.

The large oscillations in Figure 4.18 of both signals is likely due to non-perfect phase matching in the second harmonic crystal. It is an oscillation in the intensity of the second harmonic beam as the wavelength is changed.

Figure 4.20 is a graph of the absorbed fraction, $f_{abs} = \frac{I(0)-I(L)}{I(0)}$, versus laser wavelength. The area under the second peak of the reference beam is used as $I(0)$. The area under the first peak of the sample beam is used as $I(L)$. The absorbed fraction increases to 1 in the region of the Zn absorption line.

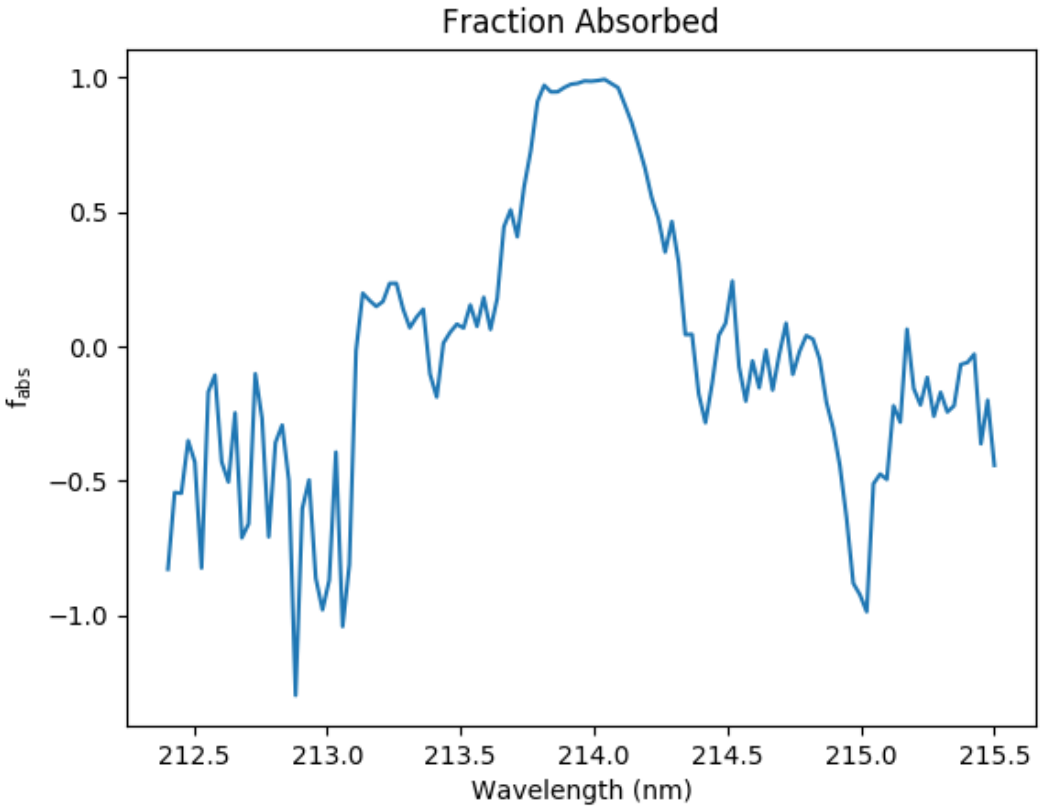

Figure 4.19: Absorbed fraction $f_{abs} = \frac{I(0)-I(L)}{I(0)}$ as a function of wavelength, where $I(0)$ is the integrated peak area of the reference beam and $I(L)$ is the integrated peak area of the sample beam.

To the sides of the absorption peak, an absorbed fraction of approximately zero is expected. But the fraction decreases to below zero on both sides of the peak. This indicates that the signal in the delayed path is smaller than the peak that goes through the heat pipe. This can be due to the experimental setup. There is beam steering due to the beam separation and it affects the delayed path more than the path that is not delayed, because the delayed path has a longer free propagation path than the beam that goes through the heat pipe. The current setup for separating the second harmonic from the fundamental causes slight beam steering when the wavelength is tuned. Beam steering for the current beam separation setup was minimised by alignment, but the steering is still present. Ideally a system of 4 Pellin-Broca prisms would be used for beam separation instead of 2 right angle prisms as discussed in Section 5.1.

Using Origin, a Gaussian and a slope that approximates the background is fit to the data, as shown in Figure 4.20 and Table 4.6. Only the data indicatd by the red squares are used for the fit, beacuse a better fit is achieved when the data on the fringes (which have large uncertainties due to beam steering) and the plateau of the peak (caused by saturation) are omitted.

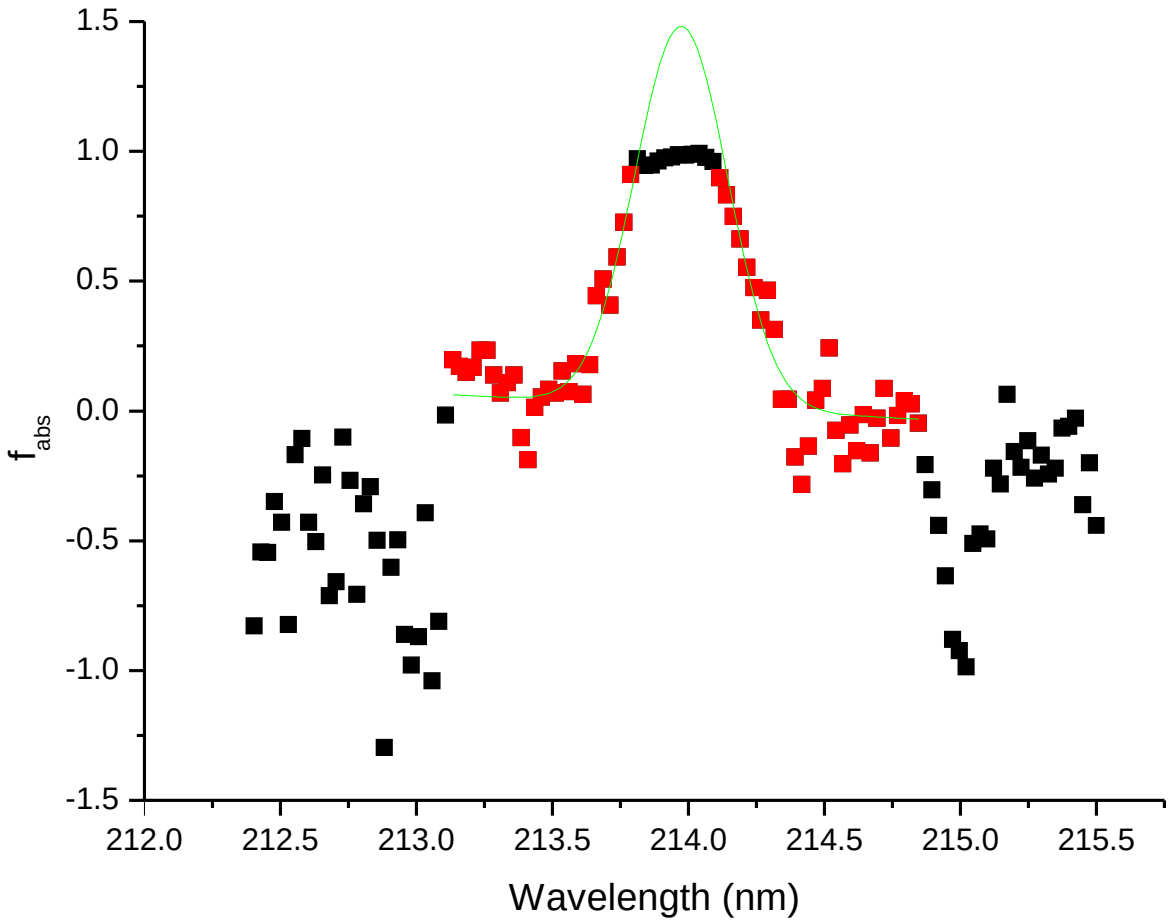

Figure 4.20: Absorbed fraction, $f_{abs} = \frac{I(0)-I(L)}{I(0)}$, where $I(0)$ is the reference and $I(L)$ is the sample signal areas. The green curve is the Gaussian fit. The red squares are the data points used for the fit. The results of the fit are shown in Table 4.6.

Equation	$y = mx + y_0 + \frac{A}{w\sqrt{\pi/2}} e^{-2((x-x_c)/w)^2}$	
Adj. R-Square	0.82763	
	Value	**Standard Error**
y_0	11.78169	7.59019
x_c	213.9742	0.14337
w	0.34203	0.02424
A	0.62827	0.10083
m	-0.05499	0.03551
$FWHM$	0.40271	

Table 4.6: Fitted values for the Gaussian fit of f_{abs} in Figure 4.20.

The Gaussian curve in Table 4.6 fits to the data with an adjusted R-Square value of

0.82763. The reason for the fit not being that good, is because of the change in the background due to slight steering of the beam as well as the plateau of the signal due to saturation.

There are two unexpected results in Figure 4.20. Firstly, the peak is not centred at 213.85735 nm as confirmed by NIST, but rather at 213.97 nm. This could be due to not enough data points or the calibration of the laser.

The other surprising feature of the peak is that it has a FWHM of 0.4 nm. The calculated transition FWHM due to Doppler Broadening is 0.0006 nm and the calculated pulse FWHM is 0.0003 nm. Together they form a Gaussian convolution with a FWHM of 0.0002 nm. In calculating the transition width, only Doppler Broadening was taken into account. There are other factors that contribute to the measured width such as the natural line width and collisional broadening. The natural line width is typically so much narrower than the Doppler broadening that is considered insignificant. The collisional broadening, however, is not so easy to calculate (as discussed in Section 2.5.3) and would also increase the FWHM. However, the most likely candidate for the increase of the FWHM is the large density of the Zn vapour. A clear sign of saturation of the peak is when there is a plateau in the peak as can be seen in Figure 4.19. For the region 213.8 nm - 214.1 nm all light is absorbed, because $f_{abs} \approx 1$ with experimental uncertainty.

The result of the measurement can be compared to the rate equation model. The transmitted intensity, $I(L)$, is calculated for the wavelengths that are changed stepwise over the resonance. This changes the value of the absorption cross-section, that is given, in the narrowband laser approximation, by $\sigma(\omega_L) = A_{21}\frac{\lambda_L^2}{4}s(\omega_L)$, where $s(\omega_L)$ is the magnitude of the line profile function at the laser wavelength.

The simulated absorbed fraction ($f_{abs} = \frac{I(0)-I(L)}{I(0)}$) is found by solving the differential equation, $\mathrm{d}I(z)/\mathrm{d}z = -\alpha(I(z), \lambda)I(z)$, where α is the intensity and wavelength dependent absorption coefficient (See Section 2.9). Figure 4.21 shows f_{abs} for different temperatures for the Zn vapour, the current laboratory value, 1060 K, the temperature needed to avoid 100% absorption, 676 K, the temperature needed for 50% absorption, 668 K and the temperature needed for significant absorption, 635 K. This gives a good indication for the working temperature for the Zn vapour for future experiments.

In Figure 4.21 the FWHM of the simulation for the current laboratory temperature of the Zn vapour, 1060 K, is 0.0025 nm. This is much smaller than the measured FWHM of 0.4 nm. This could be due to factors such as power broadening and collisional broadening as described in Section 2.5.3.

The conclusion from the experiment and simulation is that absorption spectroscopy with a delayed beam is feasible and has been demonstrated successfully.

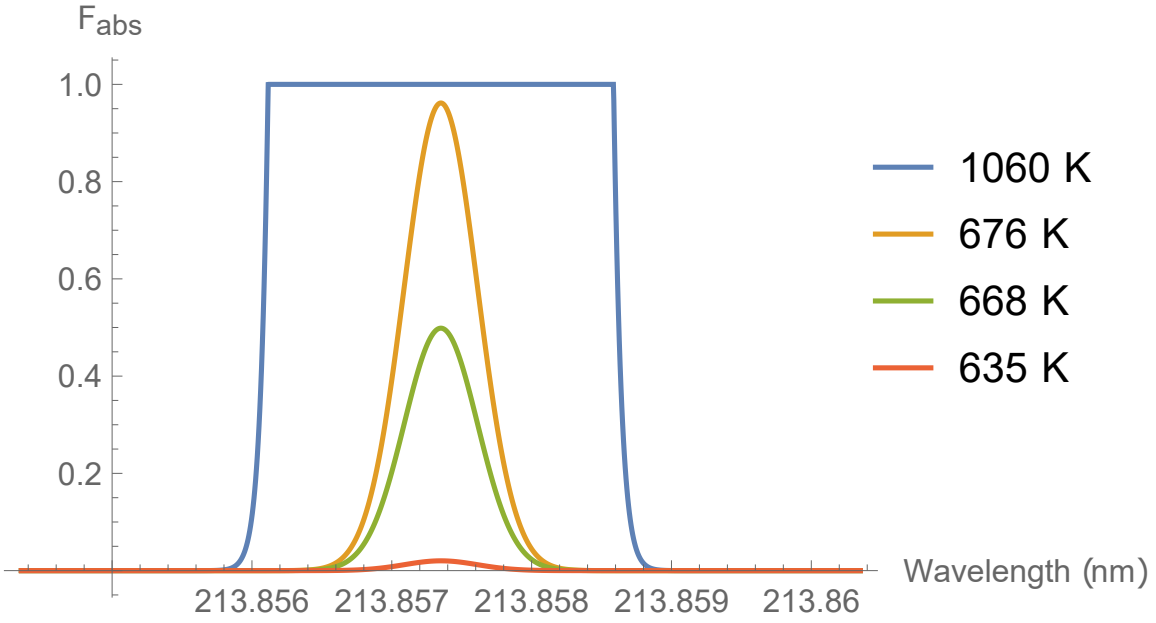

Figure 4.21: Simulated absorbed fraction, $f_{abs} = \frac{I(0)-I(L)}{I(0)}$, where $I(0)$ is the intensity of the reference beam and $I(L)$ is the intensity of the sample beam, calculated for different temperatures for the Zn vapour, the current laboratory value, 1060 K, the temperature needed to avoid 100% absorption, 676 K, the temperature needed for 50% absorption and the temperature needed for significant absorption, 635 K.

5. Conclusion

A complementary experimental setup and computational model is used to investigate the $4s^2\ {}^1S_0 \rightarrow 4s4p\ {}^1P_1{}^o$ transition of Zn, as a possible first step for ionisation. Experimental conditions are investigated through Atomic Absorption Spectroscopy (AAS) in Zn vapour as well as computationally through an Einstein rate equation model describing the interaction of atoms with incident laser beams. A computer model is used to interpret the experimental measurements and investigate the influence of experimental parameters that cannot be easily adjusted such as laser pulse duration. The computer model is also used to predict feasible experimental parameters such as the density of Zn vapour, intensity of laser beam and ionisation level scheme for future experiments.

During this project a Zn heat pipe is commissioned for AAS (See Section 3.1). The temperature, pressure and density of Zn inside the heat pipe is determined and investigated (See Section 4.3.1). A time-delayed-reference-beam absorption spectroscopy setup, with frequency doubled dye laser beams and a single detector is developed (See Section 3.4). Protocol and software are developed to analyse results of the time-delayed-reference-beam AAS setup (See Section 3.5). The first excitation step ($4s^2\ {}^1S_0 \rightarrow 4s4p\ {}^1P_1{}^o$) is detected and compared to simulated data (See Section 4.6). This transition is chosen as the first excitation step, because it has a large absorption cross-section due it being an allowed state.

The vapour pressure of the Zn vapour in the Heat Pipe is calculated to be 25 kPa at 1060 K. Using the determined temperature and pressure, the density of Zn is found to be 1.7×10^{24} atoms per m^3. A Maxwell-Boltzmann distribution is used to approximate the velocity distribution of the Zinc atoms in the Heat Pipe. Using the velocity distribution of the atoms and Doppler broadening theory, the Doppler broadened transition line width is calculated to be 2.5×10^{10} rad/s. The laser bandwidth is transformed as it undergoes Second Harmonic Generation (SHG) and is calculated to be 1.1×10^{10} rad/s.

Using the density of the atoms, the transition bandwidth and laser bandwidth, an Einstein rate equation model to model population dynamics of the ground state and the excited state of the two level system are simulated and explored (See Section 4.4). For the $4s^2\ {}^1S_0 \rightarrow 4s4p\ {}^1P_1{}^o$ transition, 5 ps is needed to reach a steady state with a constant intensity 7.5×10^8 W/m^2. The maximum intensity needed to saturate this transition when using a Gaussian with a FWHM of 8 ns is 2×10^7 W/m^2. For the $4s^2\ {}^1S_0 \rightarrow 4s4p\ {}^3P_1{}^o$ transition, 30 ns is needed to reach a steady state with a constant intensity 7.5×10^8 W/m^2. When using a Gaussian with a FWHM of 8 ns, a maximum intensity of more than 7.5×10^8 W/m^2 is needed to saturate this transition.

The absorption cross-section for the central frequency for the $4s^2\ {}^1S_0 \rightarrow 4s4p\ {}^1P_1{}^o$ transition is found to be $\sigma = 3.3 \times 10^{-16}$ m^2, using the general equation as a result of the rate equations. Using the rate equations, the fraction of absorption $f_{abs} = \frac{I(0)-I(L)}{I(0)}$ (where, $I(0)$ is the reference intensity and $I(L)$ is the sample intensity for a sample

length of L) is found to be $f_{abs} = 1 - 3.0 \times 10^{-98} \approx 1$ for a sample length $L = 0.06$ m and intensity 7.5×10^8 W/m^2. f_{abs} is plotted versus intensity and temperature and it is found that an intensity of 7.5×10^8 W/m^2 and temperature of 668 K is needed for 50% absorption ($f_{abs} = 0.5$).

Absorption was measured in a Zn vapour heat pipe in the form of $f_{abs} = \frac{I(0)-I(L)}{I(0)}$, shown in Figure 4.20. The FWHM is found to be 0.4 nm. The absorbed fraction, f_{abs}, is also simulated by solving the differential equation, $\mathrm{d}I(z)/\mathrm{d}z = -\alpha(I(z), \lambda)I(z)$, where α is the intensity and wavelength dependent absorption coefficient (See Section 2.9). Figure 4.21 shows f_{abs} for different temperatures of the Zn vapour. The FWHM of the simulation for the current laboratory temperature of the Zn vapour, 1060 K, is 0.0025 nm. This is much smaller than the measured FWHM of 0.4 nm. This could be due to factors such as saturation and collisional broadening as described in Section 2.5.3.

For future experiments, the temperature needed for 50% absorption is calculated to be 668 K.

The experimental and computational results show that absorption spectroscopy with a delayed reference beam is feasible and has been demonstrated successfully. The effect of intensity and pulse duration on the ability to saturate the transition, as well as the effect of intensity and Zn vapour density on absorbed fraction were investigated.

It is proposed that the density of the Zn vapour is decreased in future experiments. More experiments are needed to investigate the effect of spectral broadening due to high laser power and atomic collisions.

5.1 Future Work

5.1.1 Beam Separation

The current experimental setup can be improved on. At the moment the beam separation using two fused-silica prisms causes slight beam steering when scanning across different wavelengths. This can be minimised by mirroring the setup as shown in Figure 5.1. This will negate the beam steering caused by the first two prisms while still being able to separate the second harmonic beam.

An even better method (but more costly) would be to use Pellin-Broca prisms instead of right angle prisms. The Pellin-Broca prisms separate the beams by a bigger angle due to the beams travelling inside the prism for a longer distance compared to the right-angle prisms. This will allow for a cleaner separation of beams. This proposed setup is shown in Figure 5.2.

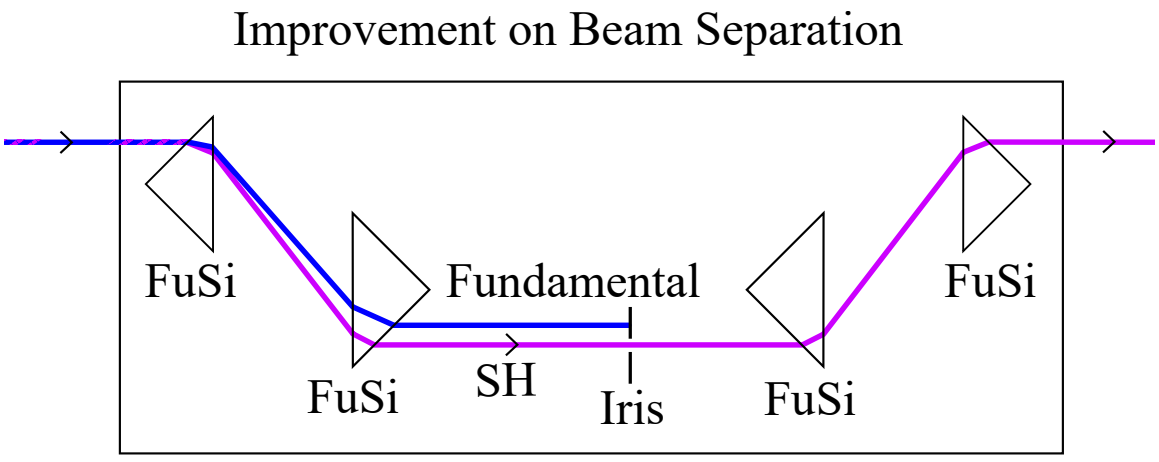

Figure 5.1: An improved beam separation that decreases the amount of steering.

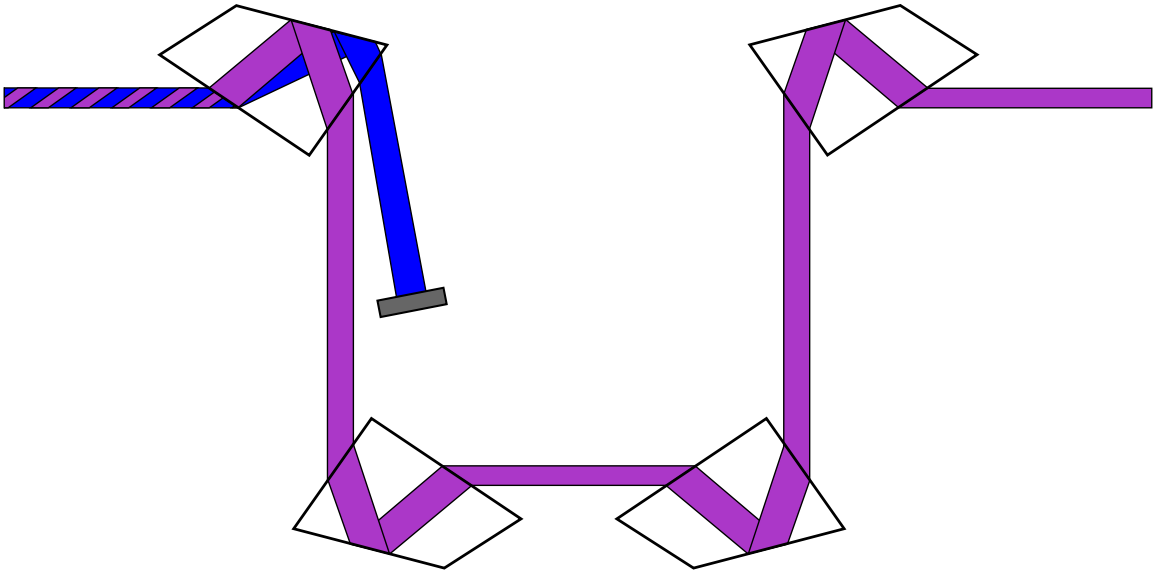

Figure 5.2: An improved beam separation that decreases the amount of steering by making use of Pellin-Broca prisms instead of right angle prisms.

5.1.2 Laser Calibration

Another improvement we can make is to re-calibrate the Lambda Physic laser closer to the wavelengths that are used. The laser was calibrated for wavelengths in the region 213.7 nm to 214 nm, but the wavelength region 212.5 nm - 215.5 nm was used for absorption measurements. A better calibration could result in more accurate measurements.

5.1.3 Beam Order

Another improvement would be to swap the beam order. As seen in Figure 4.17, even though the beams are separated by 150ns, they taper and overlap when measured on

the oscilloscope. Absorption is being measured, i.e. the decrease in the intensity of the pulse that goes through the sample, but since this signal reaches the oscilloscope first. It interfers with the second, delayed signal. The author proposes to, instead of having a delayed reference beam and a sample beam, rather have a delayed sample beam that goes through the HP and a reference beam that goes straight to the detector. This way the decrease due to absorption is in the second pulse and will not affect the first and a better absorption measurement should be obtained.

Appendices

A. Appendix

A.1 Python Code for Peak Analysis Software

```
##############################
# Peak Analysis Software
# Brandon Hattingh 2018
##############################
import numpy as np
import matplotlib.pyplot as plt
from scipy import integrate

# Put data into a convenient table and save as txt
def importtxt(filename, newfilename = 'arrangedData.txt'):
    table = []
    table.append([])

    col = 3

    prevtime = -1
    with open(filename) as f:
        for line in f:
            data = line.split(",")
            # If we are working with Andre's test files
            if len(data) == 5:
                # data[0] contains the time
                # add 3 zeros at the biginning
                if prevtime == -1:
                    table[0].append(0)
                    table[0].append(0)
                    table[0].append(0)
                # Stop adding times when it starts repeating
                if float(data[col]) < prevtime:
                    break
                # Add each time in assending order
                table[0].append(float(data[col])*1000000)
                prevtime = float(data[col])

            # If we are working with csv file from oscilloscope
            if len(data) == 6:
                # add 3 zeros at the biginning
                if prevtime == -1:
                    table[0].append(0)
                    table[0].append(0)
```

```
                    table[0].append(0)
                if float(data[col]) < prevtime:
                    break
                if float(data[col]) != prevtime:
                    table[0].append(float(data[col])*1000000000)
                    prevtime = float(data[col])

    i = 0
    with open(filename) as f:
        for line in f:
            data = line.split(",")
            # If we are working with Andre's test files
            if len(data) == 5:
                if float(data[col]) == 0:
                    i += 1
                    table.append([])
                    table[i].append(data[0])
                    table[i].append(data[1])
                    table[i].append(data[2])
                table[i].append(data[4])
            # If we are working with csv file from oscilloscope
            if len(data) == 6:
                if i == 0:
                    i += 1
                    table.append([])
                    table[1].append(0)
                    table[1].append(0)
                    table[1].append(0)
                table[1].append(data[4])

    nptable = np.transpose(table)
    nptable = np.array([[item for item in s] for s in nptable])
    np.savetxt(newfilename, nptable, fmt='%s', delimiter=',', newline='\r\n')

    np.savetxt('arrangedData2.txt', [nptable[1],nptable[2],nptable[3],\
        nptable[4],nptable[5],nptable[6]], fmt='\%s', delimiter=',',\
           newline='\r\n')
    return table;

# Plot
def plotthings(table, method = 'all'):
    plt.figure(1)
    plt.ylabel('Voltage From Oscilloscope (V)')
    plt.xlabel('time (ps)')
    plt.title('Scans')
    if method == "wl":
        tol = 0.00000001
```

```
        for a in range(len(wl1)):
            for b in range(len(wl2)):
                for c in range(len(wl3)):
                    for i in range(len(table)):
                        if (abs(float(table[i][0]) - float(wl1[a])) <= tol) &\
                        (abs(float(table[i][1]) - float(wl2[b])) <= tol) &\
                            (abs(float(table[i][2]) - float(wl3[c])) <= tol):
                            t = []
                            y = []
                            for j in range(3,len(table[0])):
                                t.append(float(table[0][j]))
                                y.append(float(table[i][j]))
                            plt.plot(t, y, label=str(wl1[a]) + "," + str(wl2[b]) +\
                             "," + str(wl3[c]))

    elif method == "c":
        for i in c:
            t = []
            y = []
            for j in range(3,len(table[0])):
                t.append(float(table[0][j]))
                y.append(float(table[i][j]))
            plt.plot(t, y)

    elif method == "all":
        #for i in range(1,len(table)):
            i = 45
        t = []
        y = []
        for j in range(3,len(table[0])):
            t.append(float(table[0][j]))
            y.append(float(table[i][j]))
        plt.plot(t, y)
        i = 70
        t = []
        y = []
        for j in range(3,len(table[0])):
            t.append(float(table[0][j]))
            y.append(float(table[i][j]))
        plt.plot(t, y)

    plt.subplots_adjust(left=0.15)
    plt.draw()
    return;

# Integrate
def integratethings(table, bgi, bgf, inti = 0, intf = 0, ratio1 = 0, ratio2 = 0,\
```

```
    domain = 'all', method = 'all'):
    print('Integrating using Simpsons method...')
    bave = []
    value = []
    for k in range(len(bgi)):
        wl = []
        for i in range(1,len(table)):
            wl.append(float(table[i][2]))
            bave.append(0)
            blen = 0.0
            for j in range(3,len(table[0])):
                if ((float(table[0][j]) >= float(bgi[k].get())) &\
                (float(table[0][j]) <= float(bgf[k].get()))):
                    bave[k] += float(table[i][j])
                    blen += 1.0
            if blen == 0:
                print("The background is out of bounds. Setting background to 0.")
                bave[k] = 0
            else:
                bave[k] = bave[k]/blen;

        value.append([])
        if method == "wl":
            tol = 0.00000001
            for a in range(len(wl1)):
                for b in range(len(wl2)):
                    for c in range(len(wl3)):
                        for i in range(len(table)):
                            if (abs(float(table[i][0]) - float(wl1[a])) <= tol) &\
                        (abs(float(table[i][1]) - float(wl2[b])) <= tol) &\
                            (abs(float(table[i][2]) - float(wl3[c])) <= tol):
                                t = []
                                y = []
                                for j in range(3,len(table[0])):
                                    if (domain == "all"):
                                        t.append(float(table[0][j]))
                                        y.append(float(table[i][j]))
                                    elif ((float(table[0][j]) >= inti[k].get()) &\
                                (float(table[0][j]) <= intf[k].get())):
                                        t.append(float(table[0][j]))
                                        y.append(float(table[i][j]))
                                value[k].append(integrate.simps(np.asarray(y)-\
                            bave[k])*(t[2]-t[1]))

        elif method == "c":
            for i in c:
                t = []
```

```
            y = []
            for j in range(3,len(table[0])):
                if (domain == "all"):
                    t.append(float(table[0][j]))
                    y.append(float(table[i][j]))
                elif ((float(table[0][j]) >= inti[k].get()) &\
                 (float(table[0][j]) <= intf[k].get())):
                    t.append(float(table[0][j]))
                    y.append(float(table[i][j]))
            value[k].append(integrate.simps(np.asarray(y)-bave[k])*\
              (t[2]-t[1]))


    elif method == "all":
        for i in range(1,len(table)):
            t = []
            y = []
            for j in range(3,len(table[0])):
                if (domain == "all"):
                    t.append(float(table[0][j]))
                    y.append(float(table[i][j]))
                elif ((float(table[0][j]) >= float(inti[k].get())) &\
                 (float(table[0][j]) <= float(intf[k].get()))):
                    t.append(float(table[0][j]))
                    y.append(float(table[i][j]))
            value[k].append(integrate.simps(np.asarray(y)-bave[k])*\
               (t[2]-t[1]))

    colors = ['C0', 'C1', 'C2', 'C3', 'C4', 'C5', 'C6', 'C7', 'C8', 'C9']
    c = colors[k\%10]
    if domain == "all":
        lines = plt.axvline(t[0])
        plt.setp(lines, color=c, linestyle='--')
        lines = plt.axvline(t[len(t)-1])
        plt.setp(lines, color=c, linestyle='--')
        plt.axvspan(t[0], t[len(t)-1], alpha=0.5, color=c)
    else:
        lines = plt.axvline(float(inti[k].get()))
        plt.setp(lines, color=c, linestyle='--')
        lines = plt.axvline(float(intf[k].get()))
        plt.setp(lines, color=c, linestyle='--')
        plt.axvspan(float(inti[k].get()), float(intf[k].get()),\
         alpha=0.5, color=c)
    lines = plt.axvline(float(bgi[k].get()))
    plt.setp(lines, color=c, linestyle='--')
    lines = plt.axvline(float(bgf[k].get()))
    plt.setp(lines, color=c, linestyle='--')
```

```
        plt.axvspan(float(bgi[k].get()), float(bgf[k].get()),
            alpha=0.5, color=c)

    plt.figure(2)
    plt.ylabel('Integrated value')
    plt.xlabel('Wavelength (nm)')
    plt.title('Integrated using Simpsons Method')
    plt.subplots_adjust(left=0.15)

    for i in range(len(value)):
        plt.plot(wl,value[i])
    plt.draw()

    for i in range(len(ratio1)):
        if (ratio1[i].get() != "") & (ratio2[i].get() != ""):
            plt.figure(3)
            plt.ylabel('Fabs')
            plt.xlabel('Wavelength (nm)')
            plt.title('Fracton Absorbed')
            legend = []

            for j in range(len(ratio1)):
                if (ratio1[j].get() != "") & (ratio2[j].get() != ""):
                    r1 = int(ratio1[j].get()[5])
                    r2 = int(ratio2[j].get()[5])
                    ratio = []
                    for k in range(len(value[0])):
                        ratio.append(1- value[r1][k]/value[r2][k])
                    plt.plot(wl,ratio)
                    legend.append(ratio1[j].get() + ' and ' + ratio2[j].get())
                    np.savetxt("ratio.txt", np.transpose([wl,ratio]), fmt='\%s',\
                     delimiter=',', newline='\r\n')
            plt.legend(legend)
            plt.draw()
            break

    return;
```

B. Appendix 2

B.1 Python Code for User Interface of Peak Analysis Software

```
##############################
# User Interface for Peak Analysis Software
# Brandon Hattingh 2018
##############################
try:
    import Tkinter as tk     ## Python 2.x
except ImportError:
    import tkinter as tk     ## Python 3.x
from analise import plotthings, importtxt, integratethings
from matplotlib.pyplot import show, close

class DestroyTest():


    def __init__(self, top):
        # create the top frame
        self.top=top
        self.top.geometry("+20+20")
        self.frame=tk.Frame(self.top)
        self.top.title("Data Analysis")

        # create variables
        self.numpeaks = tk.IntVar()
        self.numpeaks.set(1)
        self.prev_numpeaks = 1
        self.numpeaks.trace("w", lambda name, index, mode,\
            numpeaks=self.numpeaks: self.recreate())
        self.filename = tk.StringVar()
        self.integrating = tk.IntVar()

        # create the widgets for the top frame
        file_label = tk.Label(self.top, text='File Name: ')
        entry_file = tk.Entry(self.top, textvariable=self.filename)
        file_label.grid(row=1, column=0, sticky="E")
        entry_file.grid(row=1, column=1, columnspan=2, sticky="W")
        entry_file.insert(0,'hot 1508v.csv')

        execute = tk.Button(self.top, text='Execute', command = self.exe_button)
        execute.grid(row=0, column=0, columnspan=3)
```

```
int_label = tk.Label(self.top, text="Do you want to integrate? ")
int_yes = tk.Radiobutton(self.top, text="yes",\
    variable=self.integrating, value=1)
int_no = tk.Radiobutton(self.top, text="no",\
    variable=self.integrating, value=0)
int_label.grid(row=2, column=0, sticky="E")
int_yes.grid(row=2, column=1, columnspan=2, sticky="W")
int_no.grid(row=3, column=1, columnspan=2, sticky="W")

peaks_label = tk.Label(self.top, text='Number of peaks: ')
entry_peaks = tk.Entry(self.top, textvariable=self.numpeaks)
peaks_label.grid(row=4, column=0, sticky="E")
entry_peaks.grid(row=4, column=1, columnspan=2, sticky="W")

# put the frame for the peak options after the top frame
self.frame.grid(columnspan=3, padx=20, pady=20)

#create frame with peak options
self.bgi = []
self.bgf = []
self.inti = []
self.intf = []
self.bgi.append(tk.DoubleVar())
self.bgf.append(tk.DoubleVar())
self.inti.append(tk.DoubleVar())
self.intf.append(tk.DoubleVar())

title_label = tk.Label(self.frame, text='Peak 0')
int_i_label = tk.Label(self.frame, text='Start Integration:')
int_f_label = tk.Label(self.frame, text='End Integration:')
bg_i_label = tk.Label(self.frame, text='Start Background:')
bg_f_label = tk.Label(self.frame, text='End Background:')
entry_int_i = tk.Entry(self.frame, textvariable=self.inti[0])
entry_int_f = tk.Entry(self.frame, textvariable=self.intf[0])
entry_bg_i = tk.Entry(self.frame, textvariable=self.bgi[0])
entry_bg_f = tk.Entry(self.frame, textvariable=self.bgf[0])

title_label.grid(columnspan=2, row=5, column=0)
int_i_label.grid(row=6, column=0)
int_f_label.grid(row=7, column=0)
bg_i_label.grid(row=8, column=0)
bg_f_label.grid(row=9, column=0)
entry_int_i.grid(row=6, column=1)
entry_int_f.grid(row=7, column=1)
entry_bg_i.grid(row=8, column=1)
entry_bg_f.grid(row=9, column=1)
```

```
        # create variables for ratios
        self.numratio = 0

        self.ratio_label = []
        self.ratio1 = []
        self.ratio_menu1 = []
        self.ratio2 = []
        self.ratio_menu2 = []

    # define function for the button
    def exe_button(self):
        close('all')
        filenameval = self.filename.get()
        table = importtxt(filenameval)
        plotthings(table)

        if (self.integrating.get() == 1):
            integratethings(table, self.bgi, self.bgf, self.inti,\
             self.intf, self.ratio1, self.ratio2, 'notall')
        show()
        return;

    # define function that runs after changing the ratio values
    def ratio_command(self,ratio_strval,curr_ratio):
        change = False
        try:
            end = len(self.ratio1)-1
            if (self.ratio1[end].get() != "") & (self.ratio2[end].get() != ""):
                change = True
        except:
            pass

        if change:
            self.numratio += 1
            n = self.numratio
            numpeaksval = self.numpeaks.get()
            options = []
            for i in range(numpeaksval):
                options.append("Peak " + str(i))
            self.ratio_label.append(tk.Label(self.top,\
                text="Plot the ratio between"))
            self.ratio_label[n].grid(row=5+n, column=0, sticky="E")
            self.ratio1.append(tk.StringVar())
            self.ratio_menu1.append(tk.OptionMenu(self.top,\
              self.ratio1[n],... *options))
            self.ratio1[n].trace("w", lambda name, index, mode,\
```

```
            ratio1_n=self.ratio1[n]: self.ratio_command(self.ratio1[n],n))
        self.ratio_menu1[n].grid(row=5+n, column=1, sticky="W")
        self.ratio2.append(tk.StringVar())
        self.ratio_menu2.append(tk.OptionMenu(self.top,\
         self.ratio2[n], *options))
        self.ratio2[n].trace("w", lambda name, index, mode,\
           ratio2_n=self.ratio2[n]: self.ratio_command(self.ratio2[n],n))
        self.ratio_menu2[n].grid(row=5+n, column=2, sticky="W")
        self.frame.grid(row=6+n, columnspan=3, padx=20, pady=20)

# define function for creating the second batch of options
def recreate(self):
    #print('does this')
    change = False
    try:
        numpeaksval = self.numpeaks.get()
        change = True
    except:
        pass

    if change:
        if (numpeaksval > 0):
            self.frame.destroy()
            if (numpeaksval == 1):
                # try:
                    for i in range(len(self.ratio_label)):
                        self.ratio_label[i].destroy()
                        self.ratio_menu1[i].destroy()
                        self.ratio_menu2[i].destroy()
                    self.numratio = 0
                    self.ratio_label = []
                    self.ratio1 = []
                    self.ratio_menu1 = []
                    self.ratio2 = []
                    self.ratio_menu2 = []
                # except:
                #     pass
            elif (numpeaksval >= 2) & (self.prev_numpeaks == 1):
                options = []
                for i in range(numpeaksval):
                    options.append("Peak " + str(i))
                self.ratio_label.append(tk.Label(self.top,\
               text="Plot the ratio between"))
                self.ratio_label[0].grid(row=5, column=0, sticky="E")
                self.ratio1.append(tk.StringVar())
                self.ratio_menu1.append(tk.OptionMenu(self.top,\
               self.ratio1[0], *options))
```

```
            self.ratio1[0].trace("w", lambda name, index, mode,\
           ratio1_0=self.ratio1[0]: self.ratio_command(self.ratio1[0],0))
            self.ratio_menu1[0].grid(row=5, column=1, sticky="W")
            self.ratio2.append(tk.StringVar())
            self.ratio_menu2.append(tk.OptionMenu(self.top,\
           self.ratio2[0], *options))
            self.ratio2[0].trace("w", lambda name, index, mode,\
           ratio2_0=self.ratio2[0]: self.ratio_command(self.ratio2[0],0))
            self.ratio_menu2[0].grid(row=5, column=2, sticky="W")
        else:
            options = []
            for i in range(numpeaksval):
                options.append("Peak " + str(i))
            for i in range(len(self.ratio_menu1)):
                if self.ratio1[i].get() == '':
                    pass
                elif int(self.ratio1[i].get()[5]) > numpeaksval-1:
                    self.ratio1[i].set('')
                if self.ratio2[i].get() == '':
                    pass
                elif int(self.ratio2[i].get()[5]) > numpeaksval-1:
                    self.ratio2[i].set('')
                self.ratio_menu1[i]['menu'].delete(0, 'end')
                self.ratio_menu2[i]['menu'].delete(0, 'end')
                for j in range(numpeaksval):
                    self.ratio_menu1[i]['menu'].add_command\
                        (label='Peak '+str(j),command=\
                            tk._setit(self.ratio1[i], 'Peak '+str(j)))
                    self.ratio_menu2[i]['menu'].add_command\
                        (label='Peak '+str(j),command=\
                            tk._setit(self.ratio2[i], 'Peak '+str(j)))

        self.prev_numpeaks = numpeaksval

        self.frame=tk.Frame(self.top)
        self.frame.grid(columnspan=3, padx=20, pady=20)

        self.bgi = []
        self.bgf = []
        self.inti = []
        self.intf = []

        title_label = []
        int_i_label = []
        int_f_label = []
        bg_i_label = []
        bg_f_label = []
```

```
                entry_int_i = []
                entry_int_f = []
                entry_bg_i = []
                entry_bg_f = []

                for i in range(numpeaksval):
                    self.bgi.append(tk.DoubleVar())
                    self.bgf.append(tk.DoubleVar())
                    self.inti.append(tk.DoubleVar())
                    self.intf.append(tk.DoubleVar())

                    title_label.append(tk.Label(self.frame,\
                        text='Peak ' + str(i)))
                    int_i_label.append(tk.Label(self.frame,\
                        text='Start Integration:'))
                    int_f_label.append(tk.Label(self.frame,\
                        text='End Integration:'))
                    bg_i_label.append(tk.Label(self.frame,\
                        text='Start Background:'))
                    bg_f_label.append(tk.Label(self.frame,\
                        text='End Background:'))
                    entry_int_i.append(tk.Entry(self.frame,\
                        textvariable=self.inti[i]))
                    entry_int_f.append(tk.Entry(self.frame,\
                        textvariable=self.intf[i]))
                    entry_bg_i.append(tk.Entry(self.frame,\
                        textvariable=self.bgi[i]))
                    entry_bg_f.append(tk.Entry(self.frame,\
                        textvariable=self.bgf[i]))

                    title_label[i].grid(columnspan=2, row=5, column=i*2)
                    int_i_label[i].grid(row=6, column=i*2)
                    int_f_label[i].grid(row=7, column=i*2)
                    bg_i_label[i].grid(row=8, column=i*2)
                    bg_f_label[i].grid(row=9, column=i*2)
                    entry_int_i[i].grid(row=6, column=i*2+1)
                    entry_int_f[i].grid(row=7, column=i*2+1)
                    entry_bg_i[i].grid(row=8, column=i*2+1)
                    entry_bg_f[i].grid(row=9, column=i*2+1)

root=tk.Tk()

DT=DestroyTest(root)
root.mainloop()
```

Bibliography

[1] Section, I.N.D.: Live Chart of Nuclides. 2018.
Available at: `https://www-nds.iaea.org/relnsd/vcharthtml/VChartHTML.html`

[2] Saloman, E.: A resonance ionization spectroscopy/resonance ionization mass spectrometry data service. I-Data sheets for As, B, Cd, C, Ge, Au, Fe, Pb, Si and Zn. *Spectrochimica Acta*, vol. 45B, pp. 37–83, 1989.

[3] Ashworth, S.H. Brown, J.: *An Atlas of Optogalvanic Transitions in Neon.* Report ral-91-069, Rutherford Appleton Laboratory, 1991.

[4] National Physical Laboratory, Kaye and Laby Tables of Physical and Chemical Constants; Section 3.4 .4, D. Ambrose, Vapour pressures from 0.2 to 101.325 kPa. 2018.
Available at: `http://www.kayelaby.npl.co.uk/chemistry/3_4/3_4_4.html`

[5] Thomas, C.L.: USGS 2016 Minerals Yearbook Zinc [Advance Release]. 2016.

[6] K., G.: Calculations for the excitation functions of 3-26 MeV proton reactions on ^{66}Zn, ^{67}Zn and ^{68}Zn. *Applied Radiation and Isotopes*, vol. 54, pp. 311–318, 2001.

[7] J.W. Engle, E.a.: Very high specific activity $^{66/68}$Ga from zinc targets for PET. *Applied Radiation and Isotopes*, vol. 70, pp. 1792–1796, 2012.

[8] M.N., A., N., A. and S.M., Q.: Evaluation of excitation functions of the ^{68,67,66}Zn(p,xn)^{68,67,66}Ga and ^{67}Zn(p,α)^{64}Cu reactions: Validation of evaluated data through comparison with experimental excitation functions of the natZn(p,x)^{66,67}Ga and natZn(p,x)^{64}Cu processes. *Applied Radiation and Isotopes*, vol. 96, pp. 102–113, 2015.

[9] Jin Kotani, E.a.: Evaluation of diagnostic abilities of Ga-SPECT for head and neck lesions. *The Japanese Society of Nuclear Medicine*, 2008.

[10] Bohlke, J.K., de Laeter, J.R., Bievre, P.D., Hidaka, H., Peiser, H.S., Rosman, K.J.R. and Taylor, P.D.P.: Isotopic Composition of the Elements, 2001. *American Institute of Physics*, 2005.

[11] Gautier, E.A., Bavio, M.A. and Fernández, M.A.: Isotopic analysis of depleted zinc in Zn-64 using thermal ionization mass spectrometry. *Analytical Methods*, vol. 7, 2015.

[12] Johannes A. Veit, E.a.: Detection of Paranasal Ectopic AdrenocorticotropicHormone-Secreting Pituitary Adenoma by Ga-68-DOTANOC Positron-Emission Tomography - Computed Tomography. *The Laryngoscope*, vol. 123, 2013.

[13] Nabi, J.-U. and Rahman, M.-U.: Gamow-Teller strength distribution in proton-rich nucleus ^{57}Zn and its implications in astrophysics. *Astrophysics Space Sci*, vol. 332, pp. 309–317, 2011.

[14] Hecht, E.: *Optics (fifth edition)*. Pearson, 2017. ISBN 13: 978-1-292-09693-3.

[15] Martin, W. and Wiese, W.: Atomic Spectroscopy. *Web version of Chapter 10 in Atomic, Molecular, and Optical Physics Handbook, G.W.F. Drake, Ed. (AIP Press, Woodbury, NY, 1996). Minor style changes have been made in this web version.*, 1996.
Available at: `www.nist.gov/sites/default/files/documents/2016/10/03/atspec.pdf`

[16] Gullberg, D. and Litzén, U.: Accurate Measured Wavelengths of Zn I and Zn II Lines of Astrophysical Interest. *Phys. Scr.*, vol. 61, pp. 652–656, 2000.

[17] Wisniak, J.: Historical Development of the Vapor Pressure Equation from Dalton to Antoine. *Journal of Phase Equilibria*, vol. 22, no. 6, 2001.

[18] Schroeder, D.V.: *An Introduction to Thermal Physics*. Addison Wesley, 2000.

[19] Aksamija, Z. and Ravaioli, U.: Energy conservation in collision broadening over a sequence of scattering events in semiclassical Monte Carlo simulation. *Journal of Applied Physics*, vol. 105, 2009.

[20] Boyd, R.: *Nonlinear Optics (third edition)*. Academic Press, 2008. ISBN 9780123694706.

[21] Rahman, M.A. and Alghoraibi, I.: Theoretical investigation of phase-mismatched second-harmonic conversion efficiency in BBO crystal. *Optik*, vol. 161, pp. 196–203, 2018.

[22] Steck, D.A.: Quantum and Atom Optics. 0116, 24 February 2017.
Available at: `http://steck.us/teaching`

[23] List of Laser Dyes, No. 35 Stilben 3(Stilben 420). December 2018.
Available at: `https://www.radiant-dyes.com/index.php/products/laser-dyes/...list-of-laser-dyes`